Progress of Theoretical Physics, Vol. 112, No. 1, July 2004

Baryon Superfluidity and Neutrino Emissivity of Neutron Stars

Tatsuyuki TAKATSUKA[1,*] and Ryozo TAMAGAKI[2,**]

[1]*Faculty of Humanities and Social Sciences, Iwate University, Morioka 020-0066, Japan*
[2]*Kamitakano Maeda-Cho 26-5, Kyoto 606-0097, Japan*

(Received April 23, 2004)

For neutron stars with hyperon-mixed cores, neutrino emissivity is studied using the properties of neutron star matter determined under the equation of state, which is obtained by introducing a repulsive three-body force universal for all the baryons so as to assure the maximum mass of neutron stars compatible with observations. The case without a meson condensate is treated. We choose the inputs provided by nuclear physics, with a reliable allowance. Paying attention to the density dependence of the critical temperatures of the baryon superfluids, which reflect the nature of the baryon-baryon interaction and control neutron star cooling, we show what neutrino emission processes are efficient in regions both with and without hyperon mixing. By comparing the calculated emissivities with respect to densities, we can conclude that at densities lower than about 4 times the nuclear density, the Cooper-pair process arising from the neutron $^3P_2$ superfluid dominates, while at higher densities the hyperon direct Urca process dominates. For the hyperon direct Urca process to be a candidate responsible for rapid cooling compatible with observations, a moderately large energy gap of the Λ-particle $^1S_0$ superfliud is required to suppress its large emissivity. The implications of these results are discussed in the relation to thermal evolution of neutron stars.

§1. Introduction

Hyperon (Y) mixing in the core of neutron stars (NSs) seems quite natural as a manifestation of the strangeness degrees of freedom in high density baryonic matter. Hyperon mixing in neutron star matter brings about a dramatic softening of the equation of state (EOS), because a substantial part of the repulsive contributions in the nucleon sector, growing at high density, is replaced by the attractive contributions of the nucleon-hyperon (NY) and hyperon-hyperon (YY) interactions since admixed hyperons are at low density. With such a too soft EOS the resulting maximum value of the NS mass (M) becomes much smaller than the observed one, $M_{\rm obs}(\mathrm{PSR}1913+16) = 1.44M_\odot$. This crucial problem is an unavoidable feature appearing in an almost model-independent manner. To resolve this problem Nishizaki, Yamamoto and Takatsuka introduced a *repulsive part of three-body force acting universally among all baryons* (equally in the NN, NY and YY parts), in their paper here referred to as NYT02.[1] This introduction was made following the repulsive part (TNR) of the three-nucleon interaction (TNI) given by Pandharipande and his collaborators, who have shown the importance of three-body force in the nucleon system.[2),3]

*) E-mail: takatuka@iwate-u.ac.jp
**) E-mail: tamagaki@yukawa.kyoto-u.ac.jp

The observational data for the surface photon luminosities of NSs relevant to surface temperatures suggest that there are at least two classes of NSs, hotter ones and colder ones. A hyperon-mixed core affords a possibility to explain the colder class data which are lower than those given by the so-called *standard* scenario of NS cooling. In the *standard* cooling, NSs in the middle age cool slowly with the conventional neutrino emission mechanism, such as the modified Urca, bremstrahlung and plasmon decay processes. These processes take place in the NS core, whose central density is not so high for less massive NSs, because the interior composition consists predominantly of neutrons and of small fractions of protons, electrons and muons. By contrast, in the *non-standard* cooling, a very fast cooling mechanism due to the direct Urca processes acts in the possible presence of *non-standard* components, such as pion condensates, kaon condensates, admixed hyperons, high fraction protons and quarks, if the NS central density becomes sufficiently high for massive NSs. In order to explain the colder class data, we need the *non-standard* cooling scenario, and at the same time, we need some agent to suppress the enormous emissivity due to a direct Urca process. Otherwise too rapid cooling incompatible with ovbservations is realized. A most natural candidate to play this suppressive role is the baryon superfluid (SF) associated with some *non-standard* component. Such a viewpoint is traced back to the mid 1980s, when the NS surface temperature too cold to be explained with the *standard* cooling scenario was first indicated by the observation on the Vela pulsar: This finding was brought about through comparison with theoretical results obtained using the calculational code of thermal evolution which was developed to properly take into account the finite time scale of thermal conduction in the crust region.[4] Since then, in studies on various possibilities of *nonstandard* cooling agents, the following characteristic aspects have been recognized as resulting from rapid cooling almost universally unless an adopted EOS is extremely stiff or extremely soft: The sharp drop in the NS surface temperature appears at age of 10^{1-2} years and the subsequent gentle decrease appears during the stage after the core and the crust become isothermal, if suitable SF suppression is assumed to reproduce the data points of the colder class.[5)-10)] Concerning studies on NS cooling problems up to recent works, review articles are to be referred to, e.g., Refs. 11)–13).

Although candidates for the *non-standard* components are many as mentioned above, one lacking an appropriate SF cannot be a candidate. This is a key point to discriminate a real candidate among possible ones.[12),14)] In previous studies on such problems it has been discussed that nucleon matter with high proton fraction and a kaon condensate is regarded as an unlikely candidate.[14),15)] In the present study concerning the hyperon-mixed NSs, it is a crucial point whether or not the emissivity due to the hyperon direct Urca is suitably suppressed by SF energy gaps of hyperons.

In addition to the suppressive role on the neutrino emissivity, the baryon SF palys a role to accelerate the NS cooling in later stages (age $\gtrsim 10^{4-5}$ years) through reduction of specific heats of SF baryons, especially in the region where the main component (normally neutron) is in the SF state.[16)] In recent years attention has been paid to another mechanism to accelerate NS cooling, Cooper-pair process due to the neutral current of the weak interaction, originally pointed out in 1976 by

Flowers, Ruderman and Sutherland.[17] In this process a $\nu\bar{\nu}$-pair is emitted when the two SF quasi-particles are recombined into the Cooper-pair in the BCS state. Since such effect takes place in the presence of a SF whose critical temperature is higher than but rather close to the internal temperature, its contributions to the neutrino emissivity come from all density regions where such SFs exist. They are larger than the modified Urca's contributions by 1-2 orders of magnitude in many cases. If the Cooper-pair process plays a significant role, the fit to the hotter class NS data obtained using the *standard cooling* scenario may be spoiled. To avoid such a situation Yakovlev and collaborators,[18)–20)] who analyzed the NS cooling aspects in a simple model or a toy model, assumed that the maximum critical temperature of the neutron $^3P_2$ superfluid is lower than the internal temperature T, typically being $\sim 10^8$ K. We consider that such an assumption is not easily acceptable from the viewpoint of nuclear theory. Also, in order to explain the colder class NS data, they made a fine tuning to the onset density of the nucleon direct Urca process together with a critical temperature of the proton $^1S_0$ SF, whose density-dependent features are not realistic at the densities where the nucleon direct Urca process would occur. Such an approach lacking due reliance on the nuclear physics inputs seems to cause confusion in the understanding of NS cooling.[21] To study the Cooper-pair process we need to adopt nuclear physics inputs carefully chosen.

Many factors come into play in the neutrino emissivity yielded in the NS core, such as the equation of state (EOS), NS mass, composition of NS matter, neutrino emission processes and baryon superfluidity. In this paper, treating the neutrino emissivity of NSs, both with and without the hyperon-mixed core, we take the following viewpoint.

1. We study the problems on the basis of reliable information provided by nuclear physics.
2. We adopt the composition of the baryonic matter determined by the EOS called "TNI6u" constructed using NYT02 interaction model with the universal repulsive three-body force mentioned above and use the effective masses of constituent baryons resulting from this EOS. We refer to this EOS as TNI6u-EOS for short.[22]
3. We adopt the following pairing interactions. The NN potentials, AV18[23] and OPEG,[24] are chosen under a reasonable restriction among the realistic potentials reproducing the scattering phase shifts of the relevant partial waves ($^1S_0$ and $^3P_2$). As a YY interaction relevant to the $^1S_0$ state, the potential named ND soft is chosen since it is compatible with hypernuclear data.[25]
4. We pay special attention to the density dependence of the critical temperatures of realized baryon superfluids. For the temperature dependence of energy gaps, we take it into account by constructing a profile function in each pairing state which is independent of the background such as the density, the pairing interaction and the effective mass.
5. We calculate the emissivities of the following three neutrino emission processes efficient in the NS core.
   (1) The direct Urca process (DUrca): For TNI6u-EOS, because the nucleon DUrca does not occur below about 6.5 times the nuclear density, only the Y

sector contributes to DUrca. Further the hyperon DUrca is possible only in the presence of Λ. The emissivity depends strongly on whether the Λ superfluidity is realized or not. Paying attention to these points we study the hyperon DUrca process.

(2) Modified Urca process (MUrca): As a representative emissivity in the standard cooling scenario, we treat the nucleon modified Urca process, because in the normal nucleon matter its emissivity is larger by 1-2 orders of magnitude than that of the nucleon bremsstrahlung process,[13] and in the SF nucleon matter this tendency holds for the case that the proton and/or neutron SF gaps are not exceptionally small or large. We pay attention to the reduction of the emisivity due to the nucleon superfluidity.

(3) Cooper-pair process (Cpp): This acts only in the presence of SFs. Since the SFs exist for all the baryons (n, p, Λ and Σ^-), the following points are of interest: How large the total Cpp emissivity is in the realistic situation, at what density the Cpp cooling is prominent, and what baryon gives main contribution. Concerning the hyperon Cpp, we use the correct expressions for the reaction constants for hyperons based on a work by Tatsumi and the present authors (here referred to as TTT03),[26] not those taken under the mistaken argument that Λ (also Σ^0) does not couple with the neutral current, e.g., as in Refs. 27), 28) and 13).

6. Finally, we compare the emissivities and discuss all aspects of emissivities and their implications in neutron star cooling. In this paper we treat NS matter without a meson condensate. In the last part, however, we illustrate an example of the emissivity arising from charged-pion condensed matter and briefly discuss it in comparison with the emissivities treated here.

This paper is organized along the line of the approach mentioned above.[29] In §2, the basic properties contained in physical inputs are described: The equation of state, composition of NS core with hyperon mixing, baryon effective masses and chosen pairing interactions. In §3, the critical temperatures of baryon superfluids existing in the NS core under TNI6u-EOS are presented. In §4, the temperature dependence of energy gaps is treated and profile functions to describe it simply are constructed. In §5, after the emissivity of each process mentioned above is shown, comparison of the three processes is presented and discussed. The last section is devoted to summary and concluding remarks related to NS cooling.

§2. Equation of state, composition of neutron star matter, baryon effective masses and pairing interactions

2.1. *Equation of state for TNI6u and the central density-NS mass relation*

In NYT02, the EOS of Y-mixed NSs has been calculated by a G-matrix based effective interaction approach which constructs the density (ρ)-dependent effective baryon-baryon (BB) interactions $\tilde{V}_{BB}$ ($B \equiv N, Y$), supplemented by the ρ-dependent three-nucleon interaction $\tilde{V}_{\rm TNI}$ of Illinoi-group type so as to assure the saturation property of symmetric nuclear matter. Three parameters inherent in $\tilde{V}_{\rm TNI}$ are de-

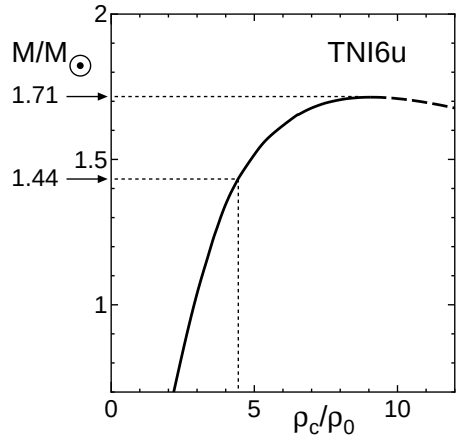

Fig. 1. Neutron star mass M as a function of central density ρ_c for TNI6u-EOS.

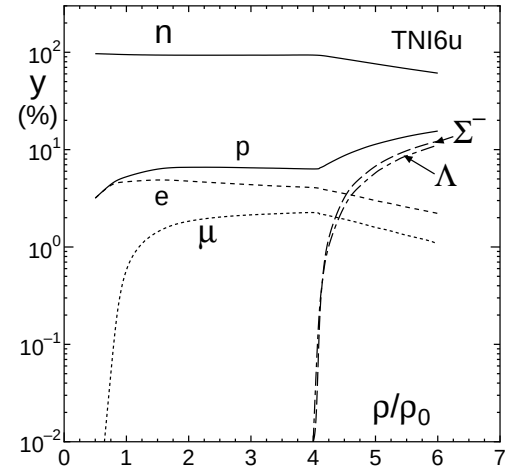

Fig. 2. Composition of neutron star matter for TNI6u-EOS; fractions y of constituent particles.

termined from the binding energy $E_B = -16.0$ MeV, the saturation density $\rho_s = \rho_0$ (the nuclear density) and a given nuclear incompressibility κ which measures the stiffness of nucleon part of EOS. Two cases for κ are considered in NYT02, $\kappa = 250$ MeV (TNI2) and $\kappa = 300$ MeV (TNI3), which lead to the maximum mass $M_{\max}$ for NS models as $M_{\max} = 1.52\ M_\odot$ (TNI2u) and $M_{\max} = 1.83\ M_\odot$ (TNI3u), respectively. The notation TNIu, instead of TNI, means that the repulsion from $\tilde{V}_{\rm TNI}$ is introduced universally for NN, YN and YY parts. If TNI is restricted to NN part, we have $M_{\max} = 1.08\ M_\odot$ (TNI2) and $M_{\max} = 1.10\ M_\odot$ (TNI3), clearly contradicting the observations ($M_{\max} < M_{\rm obs} = 1.44\ M_\odot$). As mentioned in the previous section, in the present study we adopt the EOS named TNI6u,[22] which corresponds to $\kappa = 280$ MeV and has the character intermediate between those of TNI2u and TNI3u described in NYT02, although the aspects of Y-mixed core depend weakly on the choice of EOS. Here its aspects directly related to the present study are given.

The maximum value of the NS mass (M) obtained for TNI6u-EOS is $M_{\max} = 1.71 M_\odot$, as shown in Fig. 1. If we use the TNR only for the nucleon part, $M_{\max} \simeq 1.1\ M_\odot$, which is much less than $M_{\rm obs}$. The numbers frequently referred in what follows are the central densities ρ_c corresponding to $M \sim M_{\rm obs}$. Figure 1 shows that $\rho_c \lesssim 4\rho_0$ for $M \lesssim 1.4\ M_\odot$, $\rho_c \simeq 4.5\rho_0$ for $M \simeq 1.44\ M_\odot$, and $\rho_c \gtrsim 5\rho_0$ for $M \gtrsim 1.5\ M_\odot$, where the nuclear density is taken as $\rho_0 = 0.17\ {\rm fm}^{-3}$.

2.2. *Composition of neutron star matter*

The composition of NS matter obtained under this EOS is shown by the fractions y of the constituent particles in Fig. 2. Notable aspects are as follows:

1. Mixings of Λ and Σ^- set in at almost the same density $\rho \simeq 4\rho_0$ near the central density for the NS with $M \simeq 1.4 M_\odot$. The threshold densities are $\rho_t(\Lambda) = 4.02\rho_0$ and $\rho_t(\Sigma^-) = 4.07\rho_0$. The fractions y_Λ and y_{Σ^-} increase abruptly to about 10% as $\rho \to 6\rho_0$.

2. The muon (μ^-) exists for $\rho \gtrsim 0.7\rho_0$.
3. Due to the Σ^- mixing the proton fraction y_p increases, but y_p is still low so that the nucleon direct Urca process does not act until about $6.5\rho_0$, where the relation among the Fermi momenta, $k_F(n) > k_F(p) + k_F(\ell)$, holds for $\ell = e^-$ and μ^-.[22)]

2.3. *Effective masses of relevant baryons*

The baryons existing in neutron star matter of our interest at $\rho \lesssim 6\rho_0$ are the main component, neutrons, and small components of protons, Λ and Σ^-. The effective masses of these baryons M_i^* calculated for TNI6u-EOS are shown in Fig. 3 by using the effective mass parameters $m_i \equiv M_i^*/M_i$ for $i = n,\ p,\ \Lambda$ and Σ^-, where M_i is the bare mass. As the density increases from the starting density of the liquid core ($\rho \simeq 0.5\rho_0$), both m_n^* and m_p^* at densities of interest decrease gradually. Moderately high values of m_n^* at low density and low values of m_p^* at densities of interest are due to the difference between the effects of the np interaction to the one-particle potentials. A moderately large value of $m_\Lambda \simeq 0.8$ comes from the attractive $n - \Lambda$ P-wave interaction.[30)] We see the very large value of $m^*_{\Sigma^-} \simeq 1.2 \to 1.0$ as $\rho \simeq 4\rho_0 \to 6\rho_0$, as shown in NYT02.[1)] These high effective masses of the mixed hyperons are favorable for making their energy gaps larger, if the pairing interaction is attractive enough.

2.4. *Pairing potentials adopted*

The pairing interactions needed in the present study are those in the ${}^1S_0$ state for the low density components, p, Λ and Σ^- and those in the neutron ${}^3P_2$ state (rigorously the ${}^3P_2 + {}^3F_2$ coupled state). For the NN interaction, we adopt AV18 and OPEG potentials. The AV18 potential[23)] is one of the modern potentials with 18 terms including the terms describing the charge dependence (CD). It reproduces the NN data very well. The OPEG potential,[24)] although charge-independent with 14 terms, is given in the same framework for AV18, apart from the CD terms, by rewriting definitions of angular-momentum dependent terms, and it well reproduces the solutions of the phase shift analysis (PSA). (For details, see Appendix A.)

In Fig. 4 the ${}^3P_2$ phase shifts are shown together with the solutions of the PSA.[31)−33)] The variation seen in the phase shifts for the three potentials in the inelastic region ($T_{\rm Lab} \gtrsim 350$ MeV) reflects the difference in the repulsive cores of the potentials and related changes outside the core region. The stronger the repulsive core is, the lower phase shifts becomes. OPEG-B gives the largest phase shifts very close to those obtained with the CD-Bonn potential,[34)] one of the modern potentials, shown for reference. OPEG-A gives the phase shifts between the two, AV18 and OPEG-B. We regard the hump in the solutions of the PSA above these curves at $T_{\rm Lab} \simeq 400 - 700$ MeV as a result due to the effects of the channels opened in the inelastic region, that is, these potential predictions merely represent the background phase shifts. Therefore we can say that these three potentials cover the reliable extent of the pairing potentials in this state.

In the NN ${}^1S_0$ state we adopt the potentials of AV18 and OPEG . (A and B are the same in this state.) Difference between the phase shifts in the inelastic region

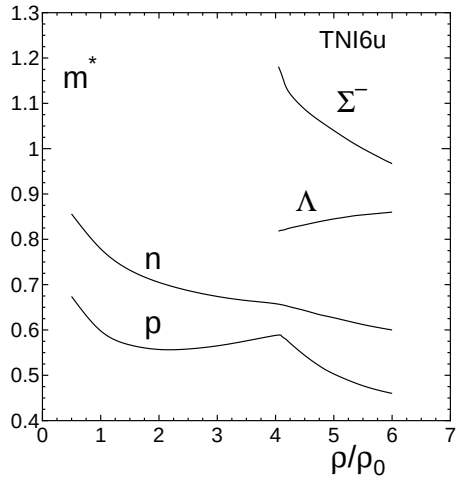

Fig. 3. Effective mass parameters of existent baryons for TNI6u-EOS.

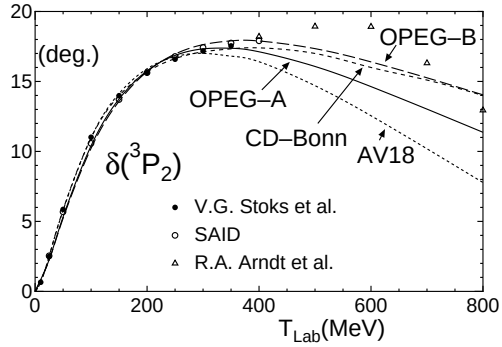

Fig. 4. The $nn\ ^3P_2$ scattering phase shifts calculated by solving the coupled equation with the $^3F_2$ state for the potentials indicated. Solutions of the phase shift analysis are shown by the marks.

given by the two is small, but AV18 gives a slightly lower phase shifts than OPEG, reflecting a little stronger repulsive core.

For the $YY\ ^1S_0$ potentials, we adopt that compatible with the available data on hypernuclei, named ND-soft,[25] which consists of a repulsive soft core and a moderate attraction weaker than the NN interaction. For other choices of YY potentials, qualitatively different results do not come about as shown in previous articles,[35)–37)] and we use preferentially the ND-soft potential here.

§3. Critical temperatures of baryon superfluids

Generally, energy gaps in the baryon superfliud (SF) are sensitive to the pairing interaction and the baryon effective mass. In this section we show the density-dependent features of the critical temperatures T_c related directly to the energy gaps, because T_c are convenient in comparison with each other for different types of energy gaps and also in direct comparison with the internal temperature T.

In calculating the energy gaps we use the effective mass approximation deduced from the single-particle potentials for each baryon in TNI6u-EOS, since we use the expressions of neutrino emissivity obtained in the approximation replacing all the quantities slowly varying near the Fermi surface by those at the Fermi surface, and the effective mass approximation is preferentially adopted in this treatment.

3.1. $^1S_0$ *superfluids of p,* Λ *and* Σ^-

For p, Λ and Σ^-, because of their small fractions, the $^1S_0$ SFs are realized for each fractional density less than about $0.5\rho_0$, with the upper limit determined mainly by the repulsive core effect. We define the effective critical temperatures $T_c^*(i)$ related to the $^1S_0$ energy gaps of the baryon (i) at zero temperature $\Delta_i(k_F, T=0)$ as

$$k_{\rm B}T_c^*(i) \equiv 0.57\Delta_i(k_F, T=0), \qquad (i = p,\ \Lambda,\ \Sigma^-) \tag{3·1}$$

where $k_{\rm B}$ is the Boltzmann constant and k_F is the Fermi momentum (i being suppressed). The quantities $T_c^*(i)$ thus defined become the starting point for studying the temperature dependence of the energy gaps, although the real critical temperature T_c is slightly shifted from $T_c^*(i)$ in most cases, as discussed in the next section.

The coefficient 0.57 on RHS of Eq. (3·1) is obtained in the well-known approximation that the gap equation with the bare $^1S_0$- pairing interaction matrix elements $\langle k'|V|k\rangle$ over the full range of the momentum,

$$\Delta(k,T) = -\frac{1}{\pi}\int k'^2 dk' \langle k'|V|k\rangle \tanh(E(k',T)/2k_{\rm B}T)\Delta(k',T)/E(k',T), \qquad (3\cdot2)$$

is replaced by the gap equation restricted to a narrow interval around the Fermi momentum k_F with effective pairing matrix elements. We call this approximation *the near-Fermi-surface approximation* (abbreviated to NFSA).*) Here $E(k,T)$ is the qausi-particle energy $E(k,T) = \sqrt{(\epsilon_k - \epsilon_F)^2 + \Delta(k,T)^2}$, where we use the effective mass (M_i^*) approximation for the single-particle energy as $\epsilon_k - \epsilon_F \simeq (k^2 - k_F^2)/2M_i^*$.

The density dependence of $T_c^*(i)$ ($i = p$, Λ and Σ^-) is shown in Fig. 5. The following features are to be noted:

1. For the proton, $T_c^*(p)$ calculated using the NN $^1S_0$ potentials of AV18 and OPEG, gradually decreasing as ρ increases, drop sharply just beyond the threshold density of Σ^-, $\rho_t(\Sigma^-) = 4.07\rho_0$, because the increase of y_p (and thus its Fermi momentum) makes the repulsive core effect stronger, in addition to the small effective mass as $m_p^* \simeq 0.6 \to 0.5$ at $\rho \simeq (4 \to 6)\rho_0$.
2. For Λ, $T_c^*(\Lambda)$ calculated using the ND-soft $\Lambda\Lambda$ potential is moderately large ($\sim 10^9$ K $\simeq 0.1$ MeV) because of the moderately large $m_\Lambda^* \simeq 0.8$, but the Λ SF exists only in the limited region $\rho \simeq (4.0 - 5.3)\rho_0$.
3. For Σ^-, $T_c^*(\Sigma^-)$ is very large ($\sim 10^9 - 10^{10}$ K) due to the large $m_{\Sigma^-}^* \simeq (1.2 \to 1.0)$ as $\rho \simeq (4 \to 6)\rho_0$.

There is room for modification from medium polarization not considered here. For the $^1S_0$ pairing in low density neutron matter in the NS crust, it has been shown that there is an effect reducing the energy gap.[38] Although a similar effect would be expected for low density p, Λ and Σ^-, medium effect on T_c^* is still an open question since they are immersed in dense neutron matter. In any case, we have $T_c^*(p) \lesssim 1\times10^9$ K for $\rho \gtrsim 2\rho_0$, which differs largely from that assumed in Refs. 18) – 20).

3.2. *Neutron $^3P_2$ superfluid*

For neutrons in the NS core ($\rho \gtrsim 0.7\rho_0$), the $^1S_0$ SF disappears due to the repulsive core effect, and the $^3P_2$ SF is realized up to several ρ_0. Among five types of possible solutions of the gap equation,[39] here the following two typical pairings with different total angular momentum components are considered: The pairing with $J = 2$, $m_J = 0$ and $J = 2$, $m_J = \pm 2$, because the former energy gap has features close to the most general type solution without a node on the Fermi surface, and the latter energy gap with the angular-momentum alignment has nodes at the poles ($\theta_k = 0,\ \pi$) on the Fermi surface.[40),41] We discriminate them with the suffix

*) The relations obtained in this approximation, which do not depend on the interval of the integration, are useful. Such relations used in this paper are summarized in Appendix B.

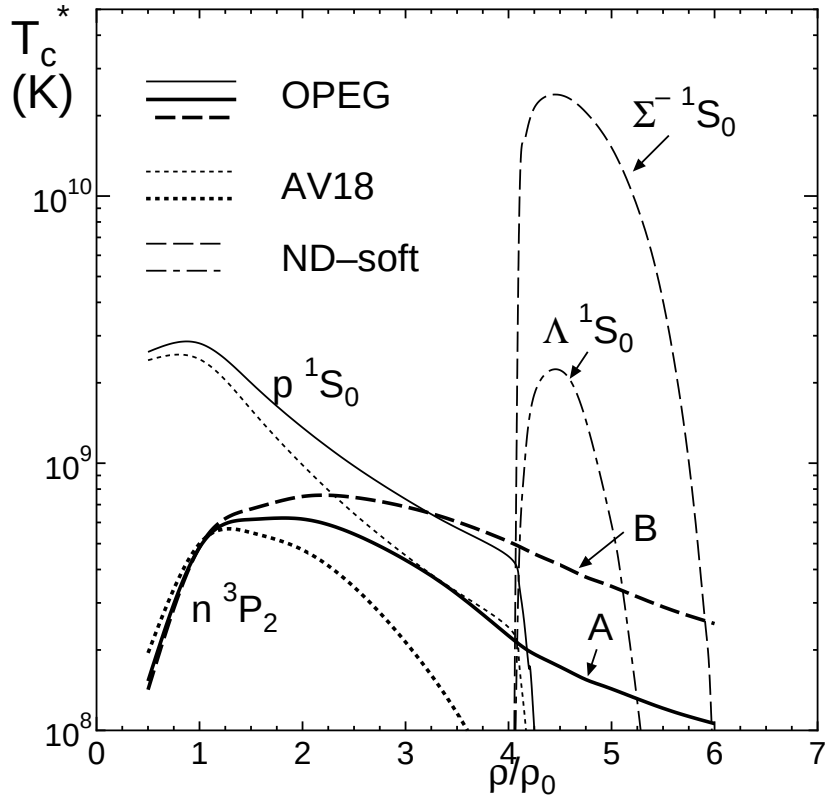

Fig. 5. Density dependence of critical temperatures T_c^* of baryon superfluids calculated with fractional densities and effective masses under TNI6u-EOS. The variation seen between the two curves for $p\ ^1S_0$ (OPEG-A and -B are the same in this state) and among the three curves for n^3P_2 mainly reflects the differences in the short-range repulsion.

$|m_J|$=0 or 2 in relevant quantities, which correspond, respectively, to B and C used in the works of Yakovlev and others.[42),13)] The two gap equations for $m_J = 2$ and $m_J = -2$ do not couple and give independent solutions with same energy gaps. The anisotropic energy gaps for the $^3P_2$ pairing are written with different angular functions $\Theta_{|m_J|}(\Omega_k)$ of the solid angle $\Omega_k = (\theta_k, \phi_k)$. In the two pairing types, the gaps are axially symmetric and depend only on θ_k.

The $^3P_2$ pairing is actually that in the $^3P_2 + {}^3F_2$ state coupled due to the tensor force. In calculations of energy gaps, we solve the coupled gap equation, and in calculations of neutrino emissivities, we use the expressions expressed in terms of the main $^3P_2$ component only. Here, first the expressions of energy gaps and critical temperatures for the single $^3P_2$ component are given and then relations to those in the coupled case are mentioned as far as necessary in the present study. As for detailed descriptions of the $\lambda \equiv {}^3P_2 + {}^3F_2$ pairing, see Refs. 43) and 44). Descriptions at finite temperature are obtained by inserting the factor $\tanh(E(\boldsymbol{k},T)/2k_BT)$ into the gap equation, where $E(\boldsymbol{k},T)$ is the quasi-particle energy with the anisotropic energy gap $D_\lambda(\boldsymbol{k},T)$, $E(\boldsymbol{k},T) = \sqrt{(\epsilon_k - \epsilon_F)^2 + D_\lambda(\boldsymbol{k},T)^2}$.

The angle-dependent energy gap $D_{|m_J|}(\boldsymbol{k},T)$ of a pure ${}^3P_2$ component, being approximatly equal to $D_\lambda(\boldsymbol{k},T)$, can be written as the following product form:

$$D_{|m_J|}(\boldsymbol{k},T) = \Delta_{|m_J|}(k,T)\Theta_{|m_J|}(\Omega_k), \tag{3·3}$$

with the angular functions

$$\Theta_0(\Omega_k) = \sqrt{(1+3\cos^2\theta_k)/2}, \tag{3·4a}$$

$$\Theta_2(\Omega_k) = \sqrt{3/2}\sin\theta_k. \tag{3·4b}$$

Here, $\Delta_{|m_J|}(k,T)$ represents the angle-averaged gap $\bar{D}_{|m_J|}(k,T)$, because

$$(\bar{D}_{|m_J|}(k,T))^2 \equiv \int \frac{d\Omega_k}{4\pi} D_{|m_J|}(\boldsymbol{k},T)^2 = \Delta_{|m_J|}(k,T)^2, \tag{3·5}$$

since the angular integral divided by 4π gives unity. According to the general prescription given in Refs. 43) and 44), $\Delta_{|m_J|}(k,T)$ are related to the gap amplitudes $\Delta^\lambda_{L,m_J}(k,T)$ as the solution of the gap equation in the ${}^3P_2+{}^3F_2$ coupled state, where $L=1$ and 3 denotes the orbital angular momenta. Extended forms of Eq. (3·5) for the energy gap $D_\lambda(\boldsymbol{k},T)$ are given by

$$(\bar{D}^{\rm coupled}_\lambda(k,T))^2 \equiv \int \frac{d\Omega}{4\pi} D_\lambda(\boldsymbol{k},T)^2 = \frac{1}{8\pi}\sum_{L=1,3}\sum_{m_J} |\Delta^\lambda_{L,m_J}(k,T)|^2, \tag{3·6}$$

which are written explicitly as sums of the ${}^3P_2$-part and the ${}^3F_2$-part. Focusing attention into the aspects near the Fermi surface and taking $k=k_F$ (the Fermi momentum of neutrons) for $m_J=0$ and $|m_J|=2$ pairings, we have

$$\begin{aligned}\bar{D}^{\rm coupled}_{\lambda m_J=0}(k_F,T) &= \sqrt{(\Delta^\lambda_{10}(k_F,T))^2+(\Delta^\lambda_{30}(k_F,T))^2}/\sqrt{8\pi} \\ &\simeq \Delta^\lambda_{10}(k_F,T)/\sqrt{8\pi}, \end{aligned}\tag{3·7a}$$

$$\begin{aligned}\bar{D}^{\rm coupled}_{\lambda |m_J|=2}(k_F,T) &= \sqrt{(\Delta^\lambda_{12}(k_F,T))^2+(\Delta^\lambda_{32}(k_F,T))^2}/\sqrt{4\pi} \\ &\simeq \Delta^\lambda_{12}(k_F,T)/\sqrt{4\pi}. \end{aligned}\tag{3·7b}$$

Here, the difference of a factor of $\sqrt{2}$ in the denominators on RHS comes from the degrees of freedom, namely, 1 (2) for the $m_J=0$ ($m_J=\pm 2$) case. These approximate expressions mean that the coupling to the ${}^3F_2$-component by the tensor force plays an important role to enlarge the main ${}^3P_2$-component, but its squared magnitude itself is much smaller than that of the main component (less than about 5% in most cases). Thus we can simply write the last expressions on RHS of Eq. (3·7) as $\Delta_{|m_J|}(k_F,T)$, corresponding to Eq. (3·3):

$$\Delta_0(k_F,T) = \Delta^\lambda_{10}(k_F,T)/\sqrt{8\pi}, \tag{3·8a}$$

$$\Delta_2(k_F,T) = \Delta^\lambda_{12}(k_F,T)/\sqrt{4\pi}. \tag{3·8b}$$

Since the actual solutions have the property at low temperature that [39)]

$$\Delta^\lambda_{10}(k_F,T) \simeq \sqrt{2}\Delta^\lambda_{12}(k_F,T), \tag{3·9}$$

the quantities $\Delta_{|m_J|}(k_F, T = 0)$ for the two types of pairing are very close, and a slightly larger value for the $m_J = 0$ pairing gap just compensates for the small difference in the coefficients of the definition of effective critical temperature T_c^* (0.60 and 0.61), which are obtained in NFSA, as given below. This feature is confirmed in numerical calculations. Thus we may take a single value for T_c^* of the neutron $^3P_2$ SF at a given density. This is quite reasonable because the critical temperature is defined as the temperature at which the energy gap vanishes, for any value of $|m_J|$. By writing k_F as $k_F(n)$, the effective critical temperature of the neutron $^3P_2$ SF can be defined from the zero temperature energy gap:

$$k_B T_c^*(n) \equiv 0.60\Delta_0(k_F(n), T = 0) \simeq 0.61\Delta_2(k_F(n), T = 0). \qquad (3{\cdot}10)$$

The values of $T_c^*(n)$ obtained by solving the $^3P_2 + {}^3F_2$ coupled gap equation for the $m_J = 0$ type pairing are shown in Fig. 5. The critical temperatures calculated using AV18 and OPEG-A & -B are of moderate magnitude, exhibiting the peak values $\simeq (6 - 8) \times 10^8$ K and decreasing gradually as ρ increases. The variety displaced by the three curves reflects the feature that the stronger the short-range repulsion, the smaller the energy gaps. We regard this extent as a reliable allowance in $T_c^*(n)$ of the core neutrons that is acceptable from the viewpoint of nuclear theory. In any case we can exclude such a possibility that $T_c^*(n) < 1 \times 10^8$ K in the NS core as assumed in Refs. 18)–20).

Next we show the effective critical temperatures of the neutron $^3P_2$ SF in pure neutron matter (abbreviated as PNM) and compare them with those in NS matter in the beta-equilibrium mentioned above. We have two aims here. Firstly, it is meaningful to compare the two, because the neutron $^3P_2$ SF plays a very important role in the neutrino emissivity, and secondly, we show the zero temperature energy gaps of this state in PNM for the OPEG-A potential, which are the revised versions of the results published in 1972, often referred to as T72. [43)]

In Fig. 6, we show the effective critical temperatures $T_c^*(n)$ versus the density obtained in PNM by solving the $^3P_2 + {}^3F_2$ coupled gap equation for the $m_J = 0$ type pairing for AV18, OPEG-A and OPEG-B potentials. The lowest curve denoted as T72 represents the results reported in T72, which should be replaced by the bold solid curve denoted as OPEG-A. The reason for the lower values in T72 is that in the 1972 work the mesh size adopted in numerical calculations was not sufficiently fine. Such a choice is found to lead to an underestimation of the energy gap in some cases, and the tendency is more pronounced as energy gaps become small.

Present calculations in PNM have been carried out by using the following effective mass parameters. With $k_F(n)$ in fm^{-1}, they are given by Lagrange's 4-point interpolation formula in the region including the points $m_n^*(k_F(n))$ =0.82(1.614), 0.78(1.915), 0.75(2.130) and 0.70(2.406), which were used in T72, and are extended to the lower and the higher regions as follows: $m_n^* = 1.03 - 0.13k_F(n)$ for $k_F(n) \leq 1.614$ and $m_n^* = 1.105 - 0.168k_F(n)$ for $k_F(n) \geq 2.406$. These effective mass parameters are a little larger than those shown in Fig. 3. This is the reason why the values of $T_c^*(n)$ in Fig. 6 are a little higher than those in Fig. 5.

Comparing the three bold curves of T_c^* in Fig. 6 with the corresponding curves shown in Fig. 5, we notice that the neutron $^3P_2$ SF in NS matter persists at higher

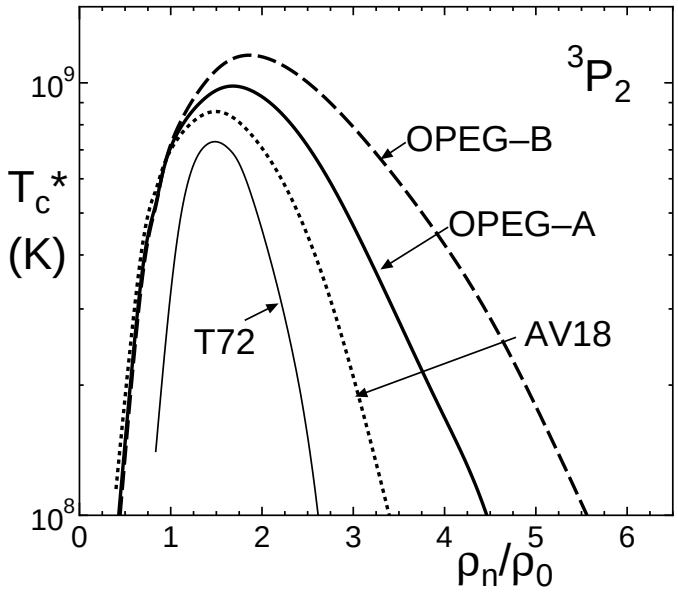

Fig. 6. Density-dependence of the effective critical temperatures T_c^* of $^3P_2$ SF in pure neutron matter for the three potentials indicated. The thin curve represents the results of T_c^* for OPEG-A given in T72.

densities than in PNM. This is because the mixing of protons and hyperons makes the neutron density lower than in PNM. The termination density of the $^3P_2$ SF in PNM for AV18 is estimated as about $3.5\rho_0$ from Fig. 6. This is almost the same as that inferred from the $T = 0$ gaps given by Baldo et al., who calculated $T = 0$ gaps in PNM by solving the $^3P_2 + {}^3F_2$ gap equation in an angle-averaged approximation for several potentials.[45] For $\rho \lesssim 3\rho_0$, T_c^* converted from their gaps are somewhat larger than those shown in Fig. 6, because values of m_n^* estimated from the single-particle potential are larger than those shown in Fig. 3.

There is still some ambiguity coming from the effects untreated here, such as effective interaction from medium polarization for the neutron $^3P_2 + {}^3F_2$ pairing. Although enhancement effect was reported earlier,[46] recently there have been reported different aspects; medium effect suppresses the $^3P_2$ gap[47], while it brings about a large P-wave pairing gap prior to the pion condensation.[48] Since these are still open problems, we regard them as to be taken into account when a problematic situation would be clear.

§4. Temperature dependence of energy gaps

Generally, the energy gap decreases smoothly as the temperature T increases and vanishes at the critical temperature T_c. Superfluids in NS matter experience a temperature change as NSs cool down. In calculations of the neutrino emissivity, we need to take into account the temperature dependence of the energy gaps of the baryon SFs as well as their density dependence shown in the previous section.

For the $^1S_0$ pairing, many investigations have been carried out for this problem, in the cases of superconductors and nucleon matter.[49),50)] Because the T dependence of the energy gap comes from the factor $\tanh(E(\boldsymbol{k},T)/2k_BT)$ in the gap equation, some common feature of the T dependence is expected, although, in principle, the details depend on the background provided by the pairing interaction, the Fermi momentum, the effective mass and so forth. If a profile function almost independent of such a background is found, it would be very useful to obtain the T dependence from the energy gap at zero temperature (equivalently the critical temperature) without solving the T-dependent gap equation many times in calculating for varying densities and temperatures in the NS interior. In what follows, we can show that this is the case. Levenfish and Yakovlev[51)] gave such a numerical fit to the T dependence of the energy gap relative to k_BT for the nucleon SFs of $^3P_2$ as well as $^1S_0$ in neutron star matter. Although their numerical fit is fairly good in a practical sense, it has some unsatisfactory features from the theoretical point of view, and yields considerably higher values near the critical temperature than the actual solutions we have calculated. In this section, we report another numerical fit for the energy gap at finite T relative to that at zero temperature. Here we present the expressions which we have chosen and used in calculations of the neutrino emissivity in the next section. Further details are given in Appendix C.

The form of the profile function we have chosen is given as a function P of the argument $\tau \equiv T/T_c$, which represents the ratio of the energy gap to the zero temperature gap and has a two-region description, the one describing the side including $T = 0$, and the other describing the side including T_c. It is given by

$$P(\tau) \equiv \Delta(k_F,T)/\Delta(k_F,T=0) \tag{4·1a}$$

$$= 1 - \sqrt{2\pi a_0 \tau}\, \exp\left[-1/(a_0\tau)\right]\ (1 + \alpha_1\tau + \alpha_2\tau^2), \quad (0 \le \tau \le \tau_b) \tag{4·1b}$$

$$= a_0 C_1 \sqrt{1-\tau}\left[1 + \beta_1(1-\tau) + \beta_2(1-\tau)^2\right], \quad (\tau_b \le \tau \le 1) \tag{4·1c}$$

where a_0, C_1, α_1, α_2, β_1 and β_2 are constants. Equation (4·1b) assures that the energy gap ratio decreases as T starts from $T = 0$.*) The constant a_0 is defined by the coefficient appearing in the definition of T_c^* in Eqs. (3·1) and (3·10) (0.57, 0.60 and 0.61, denoted by a_0^* hereafter), multiplied by T_c/T_c^*:

$$a_0 \equiv a_0^*\,(T_c/T_c^*). \tag{4·2}$$

We can take the boundary value of the two regions as $\tau_b = 0.7$. The numerical values of the other constants are selected by the fitting to the T-dependent features obtained from energy gap calculations. They are almost universal in a sense that they are almost independent of the background mentioned above. The procedure to fix the constants is as follows:

1. Among the calculated energy gaps for typical densities, we chose several points that are used to determine the constants. Actually, we chose $\tau = 0.5,\ 0.7,\ 0.9$, in addition of the trivial points $P(\tau = 0) = 1$ and $P(\tau = 1) = 0$.

*) The numerical fit given in Ref. 51) does not necessarily insure this property; the ratio exceeds unity for $\tau \lesssim 0.3$ for the pairings of $^1S_0$ and $^3P_2$ with $m_J = 0$.

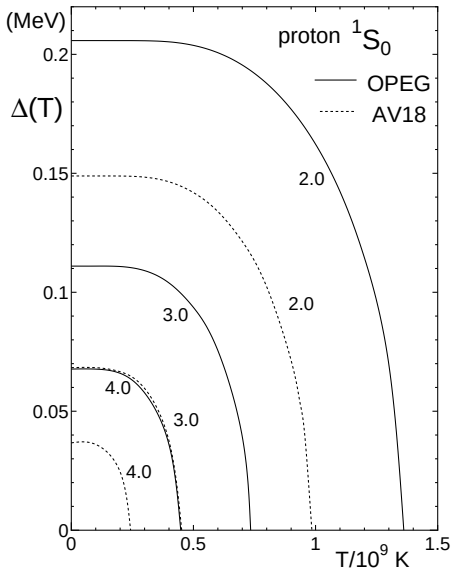

Fig. 7. Temperature dependence of proton $^1S_0$ energy gaps for $\rho/\rho_0 = 2.0, 3.0, 4.0$ in NS matter under TNI6u-EOS. the solid (dotted) curves are for OPEG (AV18).

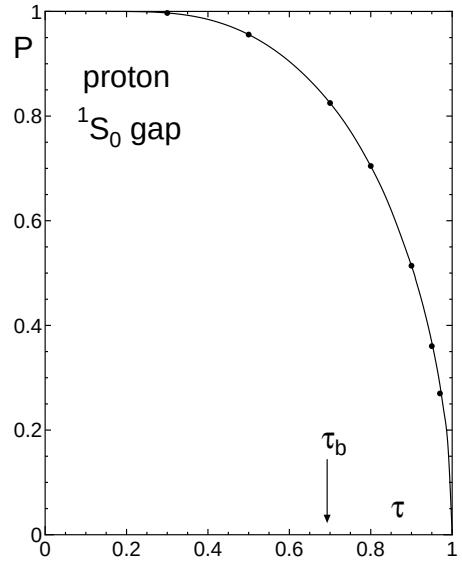

Fig. 8. Profile function $P(\tau)$ of the temperature dependence of proton $^1S_0$ energy gaps. The dots represent the average of the calculated values of $\Delta(k_F(p), T)/\Delta(k_F(p), T = 0)$ over 12 densities for each τ and the two potentials. The solid curve is the fit obtained using Eq. (4·1) and Table I.

2. We take the average and the "spread" around the average taken from all the calculated values of the gap ratio $\Delta(k_F, T)/\Delta(k_F, T = 0)$ over many densities for each τ, where the "spread" is the standard deviation assuming that these values follow a normal distribution. They are summarized in Table II in Appendix C. The calculated values are very close to each other as shown by the small spread. Because such a feature is almost independent of the pairing interactions used, we can find the same profile function for each pairing type.
3. The constants α_1 and α_2 are fixed by the fit to τ =0.5 and 0.7.
4. Using the derivative at the boundary, $\tau_b = 0.7$, obtained on the T=0 side, and the values at τ =0.7 and 0.9, C_1, β_1 and β_2 are determined. At this step, it is favorable to choose C_1 not far from the value in the limit $P(\tau \to 1) \to a_0\ C_1\ \sqrt{1-\tau}$ which is obtained in NFSA. (See Appendix B for the NFSA number.)

4.1. $^1S_0$ *pairing*

For the proton SF in NS matter, T_c obtained by solving the gap equation is very close to the effective critical temperature T_c^* defined in Eq. (3·1), which is obtained in NFSA, at densities where the SF exists and for the pairing potentials of AV18 and OPEG. Therefore, we can take the constant a_0 as $a_0 = a_0^* = 0.57$.

Examples of the T dependence of the proton $^1S_0$ energy gaps for the two potentials are shown in Fig. 7 at the three densities ($\rho/\rho_0 = 2$, 3 and 4) in NS matter under

Table I. Constants in the profile function $P(\tau)$ given by Eq. (4·1) describing the temperature dependence of the energy gaps for the pairing type listed in the first column. For the row of the neutron $^3P_2,\ m_J = 0$, T_c/T_c^* given in Eq. (4·3) is used in actual calculations, where the constants other than a_0^* are slightly changed from those in this table.

Pairing type	a_0^*	T_c/T_c^*	$C1$	α_1	α_2	β_1	β_2
Proton $^1S_0$	0.57	1.00	2.9101	−0.5435	1.5008	−0.1483	−0.5273
Neutron $^3P_2,\ m_J = 0$	0.60	1.05	2.2924	−0.2765	0.7693	0.5249	−1.6798
Neutron $^3P_2,\ \|m_J\| = 2$	0.61	1.02	1.9940	−0.2015	0.8231	1.5563	−3.3774

TNI6u-EOS, where ($k_F(p)$ in fm^{-1}, m_p^*) =(0.872, 0.557), (0.994, 0.565) and (1.085, 0.588), respectively. The averages of $\Delta(k_F(p),T)/\Delta(k_F(p),T=0)$ taken over 12 densities are represented by the dots in Fig. 8. As shown in Table II of Appendix C, the spread of deviation about the average at each value of τ is very small: less than 0.001 for $\tau \lesssim 0.8$ and less than 0.005 for $\tau \gtrsim 0.9$, for any pairing potential, which are smaller than the width of the dots in this figure. This means that a profile function $P(\tau)$ can be determined. The solid curve in Fig. 8 is the profile function of Eq. (4·1) with the constants given in Table I. The value $C_1 = 2.9101$ is slightly shifted from the value 3.06 obtained in NFSA [Eq. (B·4)], to make the fit better in the region $\tau \gtrsim 0.9$.

This profile function can be used for the Λ SF with the same order of energy gaps as in the proton case. As for Σ^- SF with the large energy gap, we may need another profile function.[37] Such problems regarding the hyperons will be reported elsewhere.[22] In this paper, we apply the $^1S_0$ profile function found in the proton case to the cases of Λ and Σ^-.

4.2. $^3P_2$ *pairing*

A typical example of the T dependence of the $^3P_2$ energy gaps is shown in Fig. 9. The density-dependent curves are $\Delta_0(k_F(n),T)$ obtained from the solutions of the coupled gap equation for $m_J = 0$ at $T = (1,3,5,8)\times 10^8$ K in PNM for the OPEG-A potential. We can see the feature that an increase of T makes the SF-existence region narrower, since it makes the gap much smaller as T approaches T_c. The same feature is found for the other potentials. If we can plot the decrease in the ratio of energy gaps for the variation of $T = 0 \to T_c$ in a manner almost independent of the background (densities, potentials, effective masses and so forth), as in Fig. 7 of the $^1S_0$ case, we could obtain a profile function of the temperature dependence of the neutron $^3P_2$ SF gaps. Actually, this is the case. We show the results in Fig. 11(a), where the solid curve is the profile function $P(\tau)$ for the $m_J = 0$ pairing, which we have obtained with use of the constants given in Table I.

The critical temperatures T_c obtained by solving the coupled gap equation for $m_J = 0$ are slightly higher than T_c^* converted from the zero temperature gaps as shown in Fig. 10: $T_c/T_c^* \simeq 1.08 \to 1.01$ as $k_F(n) = (1.2 \to 3.0)$ fm^{-1}. We should take this density-dependent feature into account in the construction of the profile function describing the T dependence of the energy gaps, and we use the equation

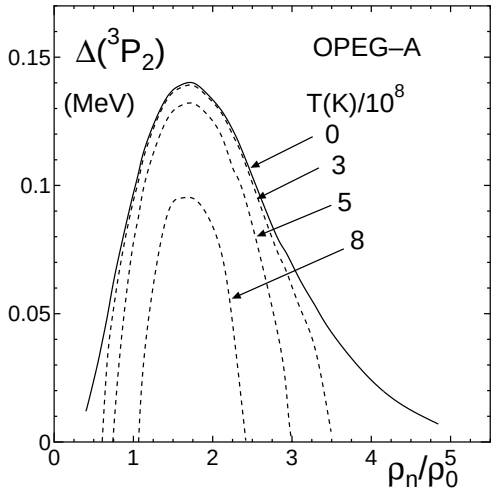

Fig. 9. Temperature variation of the density-dependence of $^3P_2$ energy gaps in pure neutron matter for the OPEG-A potential.

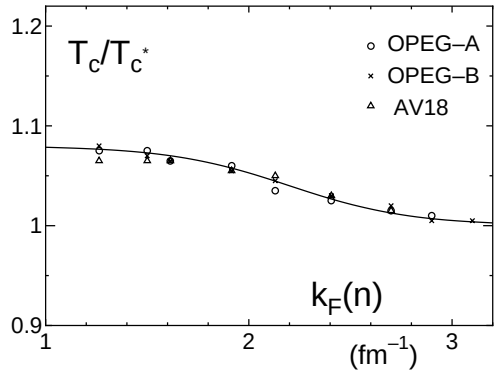

Fig. 10. Density dependence of T_c/T_c^* seen in the solutions of the $^3P_2$+$^3F_2$ coupled equation for the $m_J = 0$ pairing type in pure neutron matter for the three potentials indicated. The curve is given by Eq. (4·3).

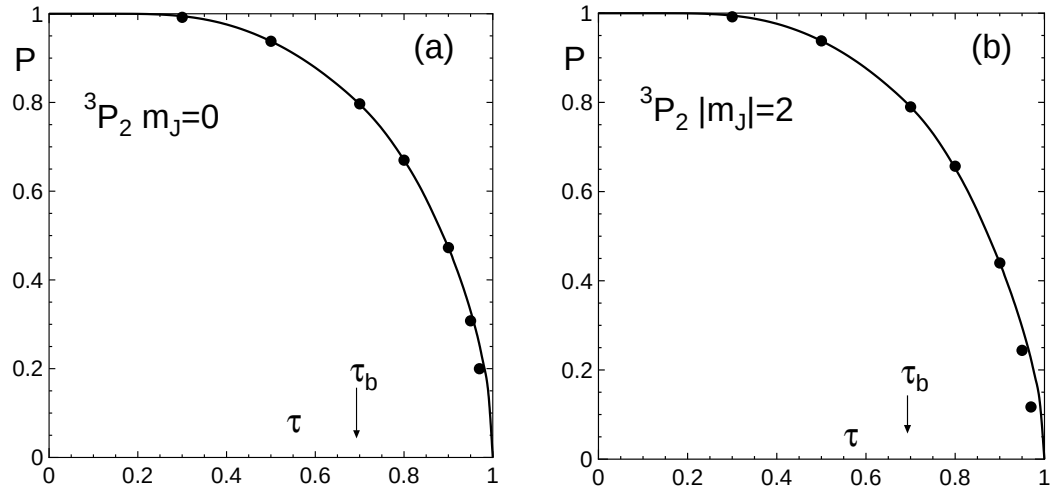

Fig. 11. Profile function $P(\tau)$ of the T dependence of the energy gaps for the neutron $^3P_2$ SF. The curves are given by Eq. (4·1). The dots represent the average at each τ for the three potentials given in Table II. (a) $m_J = 0$ pairing type with $T_c/T_c^* = 1.05$ and (b) $|m_J| = 2$ pairing type with $T_c/T_c^* = 1.02$.

$$a_0 = 0.60 \times \left\{ 1 + \frac{0.08}{1 + \exp\left[(k_F(n) - 2.2)/0.3\right]} \right\}, \tag{4·3}$$

which is shown by the curve in Fig. 10. In actual calculations of the neutrino emissivity we use this expression, although we show the profile function using the constants for $T_c/T_c^* = 1.05$ given in Table I.

We obtain a good profile function $P(\tau)$ with the numbers given in Table I, as

shown in Fig. 11(a), where the dots represent the average of $\Delta_0(k_F(n),T)/\Delta_0(k_F(n), T=0)$ calculated for 9 densities in pure neutron matter at each value of τ, for the three potentials used in the previous section. The spread of the deviation at each τ is listed in Table II of Appendix C. It is less than 0.01 for $\tau \lesssim 0.8$. For $\tau \gtrsim 0.9$, although the spreads increase, they are still not too large, and the profile function can still be used. The constant $C_1 = 2.2924$ is shifted from 2.80 [Eq. (B·5)] obtained in NFSA, to give a better fit in this region.

The same procedure can be applied for the $|m_J| = 2$ pairing. We have treated this case simply in an approximate way. Instead of solving the coupled gap equation, we multiply the tensor potential term in the uncoupled $^3P_2$ gap equation by a constant $(1+\alpha)$ with $\alpha = 0.5$ (0.47) for OPEG-A & -B (AV18), so as to reproduce the scattering phase shifts in the $^3P_2$ state.[52] The obtained profile function is plotted in Fig. 11(b), where we have used $T_c/T_c^* = 1.02$, found using gap calculations in this approximation and the constants given in Table I. A fit to the results (given in Table II and shown by the dots in this figure) with almost the same quality as in the $m_J = 0$ case is obtained. Although Yakovlev et al. used a function form with powers of τ for $|m_J| = 2$ case,[51),42)] their numerical fit to the results we have obtained by solving the gap equation is worse than the present one, especially for large τ.

We have found that the profile function of the form given by Eq. (4·1) gives a description of the temperature dependence of the energy gaps equally well for the pairings of $^1S_0$ and $^3P_2$ with $|m_J| = 0$ and 2. This fact means that the angle-average approximation works considerably well for the $^3P_2$ pairing, as long as we are concerned with the magnitude of the gap, $\Delta_{|m_J|}(k,T)$, with the property shown in Eq. (3·9).

§5. Emissivities of neutrino emission processes efficient in the core of hyperon-mixed neutron stars

In this section we study the emissivities (denoted by $\mathcal{E}$) due to three neutrino emission processes efficient in the NS core. They depend strongly on the density ρ and the internal temperature T. Our central interest is to ascertain what process plays an important role in the regions with and without hyperon mixing. In doing so, we pay attention to the strong ρ dependence of the critical temperatures of the baryon superfluids (SFs) and the T dependence of the energy gaps, obtained under TNI6u-EOS in the previous sections. For the T dependence each emissivity contains a factor representing the SF effect sensitive to the ratio Δ_i/k_BT, where Δ_i is the T-dependent energy gap, as well as the well-known factor of T^n with $n = 6-8$ specific to each process. In calculations of emissivities we take the internal temperature in the region $T \simeq (1-5)\times 10^8$ K as typical values in the NS interior of the middle-aged NSs, where the effects of nonstandard cooling and SF suppression are examined in comparison with observations.

5.1. *Direct Urca process of hyperons*

The direct Urca (abbreviated as DUrca) process in NS matter[53] is expressed as $B_1 \to B_2 + \ell^- + \bar{\nu}_\ell$ and $B_2 + \ell^- \to B_1 + \nu_\ell$ with $\ell = e,\ \mu$. We write this as

$B_1 \leftrightarrow B_2$ for short. In the baryon composition under TNI6u-EOS shown in Fig. 2, due to the momentum conservation condition, the nucleon DUrca does not occur, and the hyperon DUrca is possible only for $\Lambda \leftrightarrow p$ and $\Sigma^- \leftrightarrow \Lambda$ transitions. Here, we treat these two processes.

The formulas of neutrino emissivity due to the hyperon DUrca in hyperonic matter in the normal phase are given, e.g., by Prakash.[54] The emissivity for a specific lepton ℓ and the relevant baryons in the normal phase is given as follows: In units of erg/(cm^{3}s), we have

$$\mathcal{E}_{\rm DU} = 4.00 \times 10^{27} \left(\frac{y_e \rho}{\rho_0}\right)^{1/3} \frac{M^*_{B_1} M^*_{B_2}}{M_n^2} R(B_1 \to B_2) T_9^6 \Theta_\ell, \tag{5·1}$$

where y_e is the electron fraction, $T_9 \equiv T/10^9$ K and $\Theta_\ell = 1$ (0) for the process allowed (not allowed) by the so-called triangle condition satisfying momentum conservation. The factor $(y_e\rho/\rho_0)^{1/3}$ comes from the lepton chemical potential μ_ℓ [$\mu_\mu = \mu_e \simeq k_F(e)$]. The masses of the relevant baryons (i) in NS matter should be the effective ones, M_i^*. The quantity $R(B_1 \to B_2)$ is the ratio of the factor composed of the weak interaction coupling constants for this process to that for the $n \leftrightarrow p$ process.

For the allowed processes under TNI6u-EOS, (a) $\Lambda \leftrightarrow p$ and (b) $\Sigma^- \leftrightarrow \Lambda$, adopting the values of $R(B_1 \to B_2)$ given in Table 2 of Ref. 54), i.e. $R(\Lambda \to p)$=0.0394 and $R(\Sigma^- \to \Lambda)$=0.2055, we have the following expressions [with $T_8 \equiv T/10^8$ K]:

$$\mathcal{E}_{\rm DU}(\Lambda \leftrightarrow p) = 0.158 \times 10^{21} T_8^6 \, (y_e\rho/\rho_0)^{1/3} \times m^*_\Lambda m^*_p \left(M_\Lambda M_p / M_n^2\right) R_{AA}(\Lambda, p)(\Theta_e + \Theta_\mu), \tag{5·2a}$$

$$\mathcal{E}_{\rm DU}(\Sigma^- \leftrightarrow \Lambda) = 0.822 \times 10^{21} T_8^6 \, (y_e\rho/\rho_0)^{1/3} \times m^*_{\Sigma^-} m^*_\Lambda \left(M_{\Sigma^-} M_\Lambda / M_n^2\right) R_{AA}(\Sigma^-, \Lambda)(\Theta_e + \Theta_\mu). \tag{5·2b}$$

Both the processes for $\ell = e$ and $\ell = \mu$ are allowed above the threshold densities of Λ and Σ^-, that is, with $\rho > \rho_t(\Lambda) = 4.02\rho_0$ for (a) and with $\rho > \rho_t(\Sigma^-) = 4.07\rho_0$ for (b), and we can take $\Theta_e + \Theta_\mu = 2$ there.

For the hyperons in the SF phase, we should multiply (5·2a) and (5·b) by a reduction factor representing SF suppression effects, denoted as $R_{AA}(B_1, B_2)$, where AA means that both B_1 and B_2 are in the $^1S_0$ SF, following Levenfish and Yakovlev.[55] This is the ratio of the integral of the statistical factors in the SF phase (I_s) to that in the normal phase (I_0), $R_{AA}(B_1, B_2) \equiv I_s/I_0$. It represents the decrease of the number density around the Fermi surface due to the energy gap. We calculate it numerically as follows.

In writing the integral, we use the dimensionless energy variables, x_ν, x_ℓ, x_1 and 2, which are the energies of the neutrino, associated lepton ℓ and the two baryons (B_1, B_2) measured from the respective Fermi energy, divided by k_BT. I_s is obtained by using the distribution functions of the normal leptons, $f(x) = 1/(1+\exp(x))$, and the distribution functions of the SF baryons, $f(z_i) = 1/(1+\exp(z_i))$, for $i = 1, 2$, with the quasi-particle energy variables, $z_i \equiv \mathrm{sign}(x_i)\sqrt{x_i^2 + d_i^2}$. Here, $d_i = \Delta_i(k_F, T)/k_BT$,

where the profile function $P(\tau)$ obtained in §4 is used to describe the T dependence of the energy gap:

$$I_s = \int_0^\infty dx_\nu x_\nu^3 \int_{-\infty}^\infty dx_1 f(z_1) \int_{-\infty}^\infty dx_2 f(z_2) \int_{-\infty}^\infty dx_\ell f(x_\ell) \delta(x_\nu - z_1 - z_2 - x_\ell). \quad (5\cdot3)$$

If both baryons are normal, this integral with use of x_i in place of z_i leads to the value in the normal phase, $I_0 = 457\pi^6/5040$. If one of the baryons is normal, we can use an analytic expression for the integral over x_1 or x_2.

Sometimes, to estimate the SF suppression effect, instead of the reduction factor R_{AA}, a factor including $\exp(-\Delta_i/k_BT)$ is used. This procedure gives an overestimate of the SF suppression, compared with $R(B_1, B_2)$, if this exponetial factor only is used.[55] For the hyperon DUrca emissivities treated here, we find the following discrepancy, using the larger of the B_1 and B_2 gaps as Δ_i. For $\Delta_i/k_BT \sim (5-10)$ the procedure gives a value smaller by (1-3) orders of magnitude, and for $\Delta_i/k_BT \lesssim 4$ it gives a value smaller by several, although for $\Delta_i/k_BT \gg 1$ the emissivity is almost completely suppressed in any way.

The calculated emissivities of the two DUrca processes are shown in Fig. 12, for three temperatures, $T = (1, 3, 5) \times 10^8$ K. Under TNI6u-EOS, Λ and Σ^- appear for $\rho/\rho_0 \gtrsim 4$ and their fractions increase similarly. Of the two possible DUrca processes, the $\Lambda \leftrightarrow p$ plays a much more decisive role than the $\Sigma^- \leftrightarrow \Lambda$, because firstly $\Sigma^- \leftrightarrow \Lambda$ takes place only with the existence of Λ and secondly, the large Σ^- gap strongly suppresses $\mathcal{E}_{\rm DU}(\Sigma^- \leftrightarrow \Lambda)$. Therefore Λ plays a key role. Bearing this situation in mind, we note the following points:

1. At $T = 1 \times 10^8$ K, the strong SF suppression of $\mathcal{E}_{DU}$ imparted by the reduction factor R_{AA} appears in the range $\rho \simeq (4.2 - 4.7)\rho_0$ for the $\Lambda \leftrightarrow p$ process and in the range $\rho \simeq (4 - 5.7)\rho_0$ for the $\Sigma^- \leftrightarrow \Lambda$ process, where their values of T_c are $\gtrsim 10T$.
2. In the $\Lambda \leftrightarrow p$ process, the sharp drop of $T_c(p)$ just beyond the onset density of Λ leads to the vanishing of the proton SF suppression, except in the vicinity of $\rho = 4\rho_0$, and the SF suppression comes only from the Λ SF.
3. Even though the density region with moderately large $T_c(\Lambda) \gtrsim 5 \times 10^8$ K is included, the region in which $\mathcal{E}_{DU}(\Lambda \leftrightarrow p)$ is efficiently suppressed is rather limited, as $\rho \simeq (4 - 5)\rho_0$. If we use a more attractive $\Lambda\Lambda$ $^1S_0$ interaction such as that of Ehime or Funabashi-Gifu A potential, the SF suppression becomes stronger than presented here.[35] By contrast, if the $\Lambda\Lambda$ $^1S_0$ interaction is much weaker than this ND-soft potential, as suggested by "NAGARA" event,[56] the vanishing of the Λ energy gap results in no SF suppression to this process, and $\mathcal{E}_{DU}(\Lambda \leftrightarrow p)$ becomes very large, as shown by the flat dotted lines.
4. As T becomes higher, the SF suppression becomes less pronounced, especially for the $\Lambda \leftrightarrow p$ process, and finally tends to the limit of the normal phase, but it persists for the $\Sigma^- \leftrightarrow \Lambda$ process because of the large $T_c(\Sigma^-)$. Since the total DUrca emissivity is mainly determined by the part with the weakest SF suppression, we should consider seriously the behavior of $\mathcal{E}_{DU}(\Lambda \leftrightarrow p)$.
5. The vanishing of the Λ SF brings about a too rapid cooling of NSs incompatible with observations, if the mass of NS is large enough to include a hyperon-mixed

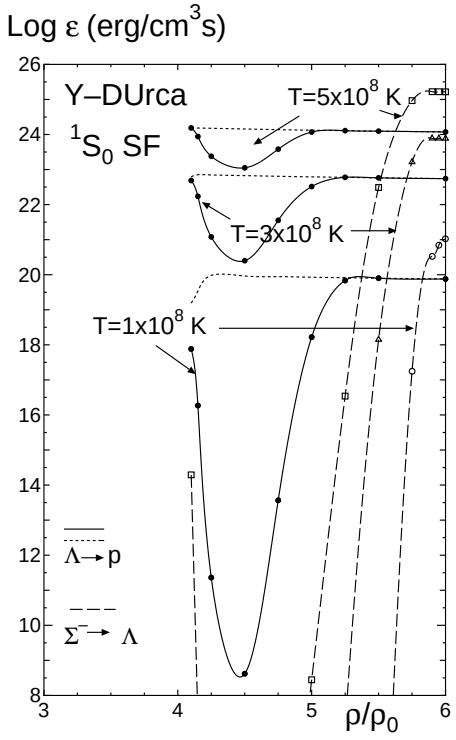

Fig. 12. Hyperon DUrca emissivities (in a log scale) of the $\Lambda \leftrightarrow p$ and $\Sigma^- \leftrightarrow \Lambda$ processes with SF suppression due to the $^1S_0$ energy gaps calculated from the ND-soft potential, at the three temperatures indicated. The dotted curves show the emissivities of $\Lambda \leftrightarrow p$ process for the case in which Λ is in the normal state.

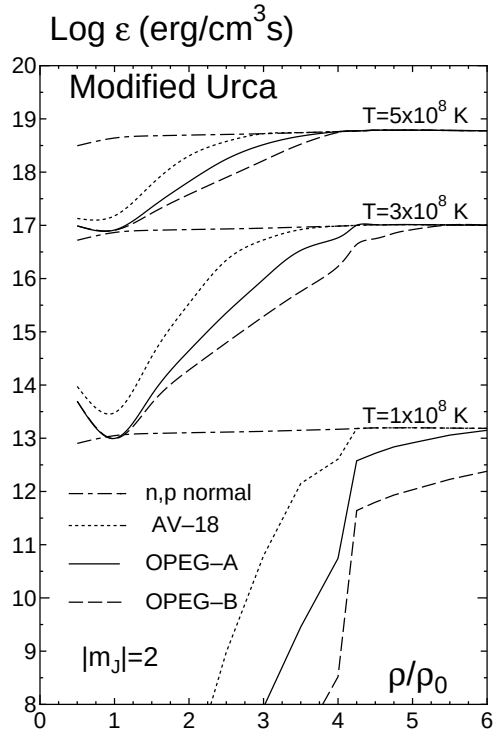

Fig. 13. Emissivities (in a log scale) of nucleon modified Urca process with SF suppression due to the neutron $^3P_2$ for $|m_J| = 2$ and proton $^1S_0$ energy gaps calculated from the three potentials and at the three temperatures, indicated in the figure. The dash-dot curves show the emissivities for both n and p being in the normal state.

core of considerable size, e.g., larger than about $1.5M_\odot$, with central density $\rho_c \simeq 5\rho_0$. *Nonstandard* cooling due to the hyperon DUrca compatible with observations is possible if a limited region of the central core of NSs contains admixed Λ with moderately large SF gaps. In this sense, the hyperon-mixing effects on NS cooling strongly depend on NS masses.

6. In summary, the key point relevant to the *nonstandard* cooling of NSs with a hyperon-mixed core is the magnitude of $T_c(\Lambda)$ provided by the attractive nature of the $\Lambda\Lambda$ $^1S_0$ interaction. This problem is intimately linked to hypernuclear physics.

5.2. *Modified Urca process of nucleons*

Modified Urca (abbreviated as MUrca) process of nucleons, which plays important roles in the *standard* cooling scenario, is expressed as $n+B \to p+B+\ell^-+\bar{\nu}_\ell$ and $p+B+\ell^- \to n+B+\nu_\ell$ with $\ell = e,\ \mu$, where B represents a bystander baryon. Here we treat the most efficient case in which $B = n,\ p$. Many authors already studied

the emissivity of the MUrca process, which provides a standard of comparison for the emissivities of various processes.[12),13),42)] The formulas for the emissivity, $\mathcal{E}_{\rm MU}$, are given by a product of the value in the case that all the associated nucleons are in the normal phase (denoted by the suffix 0) and a reduction factor describing the suppression due to the superfluidity of nucleons (denoted by R). For the former part, we use the results obtained in the model describing the momentum transfer between the associated two nucleons with one pion exchange, which was studied by Friman and Maxwell[57)] and is referred to in a recent review article.[13)] $\mathcal{E}_{\rm MU}$ consists of the sum of two contributions for $B = n$ and for $B = p$, which are called the "neutron branch" and the "proton branch".

The emissivities for nucleons in the normal phase and $\ell = e$ are given as follows, when the momentum conservation condition is satisfied in addition to the β-equllibrium condition, $\mu_\ell = \mu_n - \mu_p$. The expression for the neutron branch $\mathcal{E}^{(n)}_{0,e}$ is valid under the condition $k_F(n) > k_F(p) + k_F(e)$, implying that the nucleon DUrca process does not occur. This is satisfied for $\rho \lesssim 6.5\rho_0$ in the case of TNI6u-EOS. The expression $\mathcal{E}^{(p)}_{0,e}$ for the proton branch holds under the condition $k_F(n) < 3k_F(p) + k_F(e)$, which is satisfied for the Fermi momenta obtained from TNI6u-EOS, in addition to $k_F(n) > k_F(p) + k_F(e)$. In units of erg/(cm^{3}s), we have

$$\mathcal{E}^{(n)}_{0,e} \simeq 8.1 \times 10^{21} (m^*_n)^3 m^*_p (\rho y_p/\rho_0)^{1/3} T_9^8 C^{(n)}_{\rm MU}, \tag{5·4a}$$

$$\mathcal{E}^{(p)}_{0,e} \simeq \mathcal{E}^{(n)}_{0,e} (m^*_p/m^*_n)^2 R_F(n,p,e) (C^{(p)}_{\rm MU}/C^{(n)}_{\rm MU}), \tag{5·4b}$$

where $C^{(n)}_{\rm MU}$ and $C^{(p)}_{\rm MU}$ are the correction factors, including short-range correlation effects, which we take as 0.77.[42)] The factor $R_F(n,p,e)$ represents the ratio of the angular integral for the proton branch to that for the neutron branch, appearing in the phase space calculation:[13)] $R_F(n,p,e) = (3k_F(p) + k_F(e) - k_F(n))^2/8k_F(p)k_F(e)$ for $3k_F(p) < k_F(n) + k_F(e)$ holding at low and intermediate densities ($\rho \lesssim 4.25\rho_0$), and otherwise $R_F(n,p,e) = (3 - k_F(n)/k_F(p))/2$ (for $\rho \gtrsim 4.5\rho_0$), where the density boundary is for TNI6u-EOS. The factor $(m^*_p/m^*_n)^2$ is about 0.6-0.7 and the factor $R_F(n,p,e)$ changes as $\simeq 0.2 \to 0.7$ for $\rho \simeq \rho_0 \to 6\rho_0$. Then the product of the two factors reduces $\mathcal{E}^{(p)}_{0,e}$ as $\simeq 0.15 \to 0.5$, compared with $\mathcal{E}^{(n)}_{0,e}$. Although the MUrca emissivity in the proton branch in the normal matter is moderately suppressed at low density, stronger suppression comes from the nucleon SF, as given below.

The total MUrca emissivity in the presence of the nucleon SF is represented as

$$\mathcal{E}_{{\rm MU},e} = \mathcal{E}^{(n)}_{{\rm MU},e} + \mathcal{E}^{(p)}_{{\rm MU},e}, \tag{5·5a}$$

$$\mathcal{E}^{(n)}_{{\rm MU},e} = \mathcal{E}^{(n)}_{0,e} R^{(n)}_{A|m_J|}, \tag{5·5b}$$

$$\mathcal{E}^{(p)}_{{\rm MU},e} = \mathcal{E}^{(p)}_{0,e} R^{(p)}_{A|m_J|}, \tag{5·5c}$$

where $R^{(n)}_{A|m_J|}$ and $R^{(p)}_{A|m_J|}$ are the reduction factors due to the proton $^1S_0$ SF and the neutron $^3P_2$ SF with $|m_J|$, for the neutron branch and the proton branch,

respectively.*) For descriptions of these reduction factors, we use the approximate numerical fit recently obtained by Gusakov.[58] We note that $R^{(p)}_{A|m_J|}$ is substantially smaller than $R^{(n)}_{A|m_J|}$, and this difference is pronounced at lower densities [$\rho \lesssim 3\rho_0$ where $T_c(p) \gtrsim T_c(n)$] and lower temperatures.

The presence of the muon in NS matter causes a contribution to the nucleon MUrca emissivity, because the process occurs when the muon begins to appear (except just beyond the muon threshold density near $0.7\rho_0$). The emissivities for the $\ell = \mu$ and the normal nucleons are expressed as the ratio to the $\ell = e$ case:

$$\mathcal{E}^{(n)}_{0,\mu} \simeq \mathcal{E}^{(n)}_{0,e}(k_F(\mu)/k_F(e)), \tag{5·6a}$$

$$\mathcal{E}^{(p)}_{0,\mu} \simeq \mathcal{E}^{(p)}_{0,e}\,[R_F(n,p,\mu)/R_F(n,p,e)]\,(k_F(\mu)/k_F(e)). \tag{5·6b}$$

The factor $(k_F(\mu)/k_F(e)) = (y_\mu/y_e)^{1/3}$ represents the suppressive effect coming from the muon mass much larger than the electron mass which restricts the available momentum space, especially at low density, while the chemical equilibrium condition is the same for $\ell = e$. The ratio $[R_F(n,p,\mu)/R_F(n,p,e)]$ is slightly smaller than (equal to) unity for $\rho \lesssim 4\rho_0$ ($\rho \gtrsim 4.5\rho_0$). Because the SF reduction factors are the same as in the $\ell = e$ case, the muon contribution is expressed in the same form as $\mathcal{E}_{\mathrm{MU},e}$. Thus the total emissivity of the nucleon DUrca is given by

$$\mathcal{E}^{\mathrm{total}}_{\mathrm{MU}} = \mathcal{E}_{\mathrm{MU},e} + \mathcal{E}_{\mathrm{MU},\mu} \simeq \mathcal{E}_{\mathrm{MU},e}(1 + (y_\mu/y_e)^{1/3}). \tag{5·7}$$

From the lepton fractions shown in Fig. 2, the muon contribution is suppressed just above the muon threshold, but the total emissivity in $npe\mu$ matter quickly approaches 1.7-1.8 times that in npe matter.

Our main interest on the nucleon modified Urca process is to see the density dependence and the temperature dependence of the SF suppression effects on $\mathcal{E}_{MU}$ when the physical inputs obtained for TNI6u-EOS and the realistic pairing potentials chosen in §2.4 are used. In Fig. 13 the calculated results for the density dependence of the MUrca emissivities are shown for the $|m_J| = 2$ case, at three temperatures [$T = (1, 3, 5) \times 10^8$ K] and for three potentials (AV18, OPEG-A and OPEG-B) as an example. Qualitatively different aspects are not seen for the $m_J = 0$ case. Comparing $\mathcal{E}_{\mathrm{MU}}$ with the dash-dot-curves for the case in which both neutrons and protons are in the normal phase, the following points are noted:

1. At $T = 1 \times 10^8$ K, the SF suppression of $\mathcal{E}_{\mathrm{MU}}$ appears strongly for $\rho \lesssim 3\rho_0$ where the critical temperatures of the neutron $^3P_2$ SF and the proton $^1S_0$ SF are moderately large, as $T_c \gtrsim 5T$. As T increases, the SF suppression becomes more gradual.
2. The variation for different NN potentials faithfully reflects the magnitude of the critical temperatures shown in Fig. 5: As the short-range repulsion becomes stronger, T_c decreases, and thus the SF suppression becomes weaker.
3. Because $\mathcal{E}_{\mathrm{MU}}$ is not large and, further, the SF makes it less efficient, the emissivity of the MUrca process of nucleons is small.

*) $R^{(i)}_{A|m_J|}$ with $|m_J| = 0$ ($|m_J| = 2$) are the same as $R^{(i)}_{AB}$ ($R^{(i)}_{AC}$) for $i = n,\ p$ in Refs. 42) and 58).

5.3. *Cooper-pair process*

Cooper-pair process (abbreviated as Cpp) caused by the neutral current of the weak interaction is described as the process of neutrino pair emission when two excited SF quasiparticles are recombined into the Cooper pair in the BCS state. The importance of this process pointed out already in 1976 [17] has been overlooked for a long time. In recent years, it has attracted much attention as a candidate to make the neutrino emissivity larger than the modified Urca emissivity. [59),60)] Here we recapitulate the formula we use in the calculations, following the paper by Yakovlev, Kaminker and Levenfish, who made the formulation applicable to the $^3P_2$ SF(denoted as YKL99). [28)] The unique feature of Cpp lies in the effect appearing only in the presence of the SF. Because the dominant contribution comes from the neutron $^3P_2$ SF, and also there is some problematic point concerning the hyperon sector in the description of YKL99, we treat the nucleon sector and the hyperon sector separately, after mentioning common parts in the formula.

5.3.1. Formula for neutrino emissivity of the Cooper-pair process

The emissivity of Cpp arising in the i-th baryon SFs is written as [in units of erg/(cm^{3}s)]

$$\mathcal{E}_{\rm Cpp}(i) = 1.17 \times 10^{21} T_9^7 \; m_i^* \frac{k_F(i)}{M_i c} N_\nu R(i), \tag{5·8}$$

where the nonrelativistic approximation is taken for the baryon part, and $N_\nu = 3$ is the number of the associated neutrinos ($\ell = e,\ \mu,\ \tau$). $R(i)$ is a dimensionless factor that contains the information concerning the coupling coefficients, transition matrix elements and Fermion distribution functions. Although it gives the SF suppression when the critical temperature $T_c(i)$ is much larger than the internal temperature T ($T_c(i) \gtrsim 10\ T$), it brings about some enhancement due to the SF when the critical temperature $T_c(i)$ is not so large in comparison with T ($T < T_c \lesssim 5\ T$). We have

$$R(i) = \frac{1}{8\pi} \int d\Omega_k \int_0^\infty dx \frac{z^6}{(\mathrm{e}^z + 1)^2} (C_V(i)^2 I_{00} + C_A(i)^2 I), \tag{5·9}$$

where Ω_k is the solid angle necessary to describe the anisotropic energy gaps appearing for the $^3P_2$-pairing, z is the quasi-particle energy divided by $k_B T$, the quantities $C_V(i)$ ($C_A(i)$) are the coupling coefficients of the i-th baryon with the neutral current of the vector (axial-vector) interaction, and I_{00} and I are the quantities given by the u, v factors used in the pairing theory. Note that these quantities depend on the associated baryon i, although this specification is often suppressed to simplify the expressions, if evident. Denoting the baryon momentum by $\boldsymbol{k}$ and the baryon chemical potential by μ_i, we have

$$z = \sqrt{x^2 + d_i^2}, \quad \text{with } \ x \equiv (\epsilon_k - \mu_i)/k_B T, \tag{5·10}$$

where d_i is the temperature-dependent gap divided by $k_B T$. Hereafter, in the integral over x we take the approximation that integrands that are slowly varying around $k_F(i)$ are replaced by the values at $k_F(i)$.

For the $^1S_0$-pairing with an isotropic gap, $d_i,\ z,\ I_{00}$ and I are angle-independent. The axial-vector term vanishes because I contains factors $2(u_k v_{k'} - v_k u_{k'})^2$ which

are vanishingly small for $k \simeq k' \simeq k_F(i)$. The vector term with I_{00} contains the factors $2(u_k v_{k'} + v_k u_{k'})^2$ which are nonvanishing. We have $I_{00} = 8u_k^2 v_k^2 = 2d_i^2/z^2$ and $I = 0$, and thus

$$R(i) = C_V(i)^2 F_s(i), \quad F_s(i) \equiv d_i^2 \int_0^\infty dx \frac{z^4}{(\mathrm{e}^z+1)^2}, \tag{5·11}$$

where $d_i = \Delta_i(k_F, T)/k_B T$.

For the ${}^3P_2$-pairing, d_i, z, I_{00} and I are angle-dependent, and are given by $I_{00} = 8u_{\boldsymbol{k}}^2 v_{\boldsymbol{k}}^2 = 2d_i^2/z^2$ and $I = 16u_{\boldsymbol{k}}^2 v_{\boldsymbol{k}}^2 = 4d_i^2/z^2$. Thus, we have

$$R(i) = (C_V(i)^2 + 2C_A(i)^2) F_t(i), \quad F_t(i) \equiv \frac{1}{4\pi} \int d\Omega_k \, d_i^2 \int_0^\infty dx \frac{z^4}{(\mathrm{e}^z+1)^2}, \tag{5·12}$$

where $d_i = D_{|m_J|}(k_F, \Omega_k, T)/k_B T$ with use of Eqs. (3·3) and (3·4).

In YKL99, these two relations are expressed in a unified manner with use of $a(i)$, named the reaction constants, as $R(i) = a(i)F(i)$:

$$a(i) = C_V(i)^2, \qquad F(i) = F_s(i) \text{ for } {}^1S_0\text{-pairing}, \tag{5·13a}$$

$$a(i) = C_V(i)^2 + 2C_A(i)^2, \quad F(i) = F_t(i) \text{ for } {}^3P_2\text{-pairing}. \tag{5·13b}$$

As already noted in Ref. 17), the function $F(i)$ is sensitive to d_i: It increases steeply from 0, reaches its peak value $\simeq 4.3$ at $d_i \simeq 3.0$, diminishes in a manner like exponential decay and fades away for $d_i \gtrsim 10$. Thus the emissivity is very sensitive both to the energy gap and T. This is the most important feature in Cpp. In the absence of SF for $T_c(i) \leq T$, the function $F(i)$ is to be taken as zero.

5.3.2. Nucleon sector

The reaction constants for the proton and neutron, $a(n)$ and $a(p)$ we use are the same in the vector part but numerically different in the axial vector part, compared with those in Table 1 of YKL99. We take the vector coefficients as $C_V(n) = -1$, $C_V(p) = 1 - 4\sin^2\theta_W = 0.08$ (θ_{W} being the Weinberg angle with $\sin^2\theta_W$=0.23) and the axial vector coefficients as $C_A(n) = -g_A + \Delta\Sigma = -1.14$ and $C_A(p) = g_A + \Delta\Sigma = 1.40$, where $g_A = 1.27$ and $\Delta\Sigma = 0.127$. Here $\Delta\Sigma$ represents the shift from the SU(3) value, which is inferred from the nucleon spin problem, as studied in TTT03.[26)]

Using the values given above, we have

$$a(n) = 1, \quad a(p) = (1 - 4\sin^2\theta_W)^2 = 0.0064 \quad \text{for } {}^1S_0\text{-pairing}, \tag{5·14a}$$

$$a(n) = 1 + 2C_A(n)^2 = 3.60,$$

$$a(p) = (1 - 4\sin^2\theta_W)^2 + 2C_A(p)^2 = 3.93 \quad \text{for } {}^3P_2\text{-pairing}. \tag{5·14b}$$

The notable property here is the very small reaction constant for the proton SF of the ${}^1S_0$-pairing, which implies a small contribution from the proton SF to $\mathcal{E}_{\mathrm{Cpp}}$. The neutron ${}^3P_2$-pairing SF contributes largely to $\mathcal{E}_{\mathrm{Cpp}}$ because the reaction constant is of order of unity.

$\mathcal{E}_{\mathrm{Cpp}}$ from the neutron ${}^3P_2$ SF The Cpp emissivity in the neutron ${}^3P_2$ SF is given as [in units of erg/(cm^{3}s)]

$$\mathcal{E}_{\mathrm{Cpp}}(n) = 3.07 \times 10^{14} T_8^7 (k_F(n)/\mathrm{fm}^{-1}) m_n^* F_t(n), \tag{5·15}$$

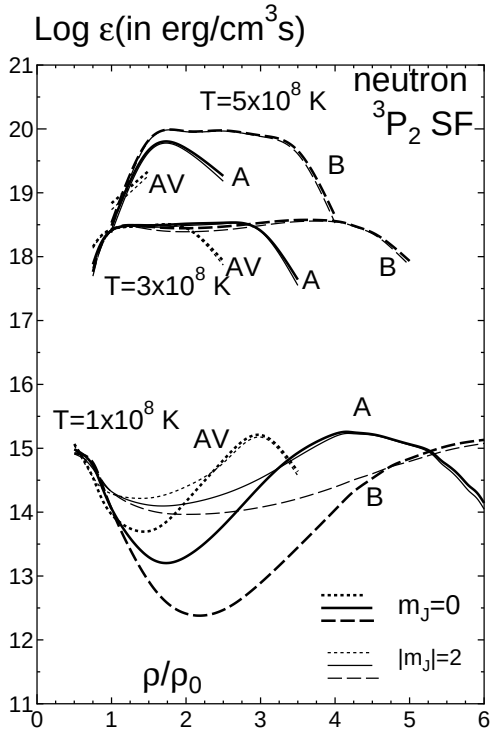

Fig. 14. Emissivities of the Cooper-pair process arising in the neutron $^3P_2$ SF for $m_J = 0$ and $|m_J| = 2$ pairing at three temperatures. The curves with AV, A and B are for AV18, OPEG-A and OPEG-B potentials, respectively.

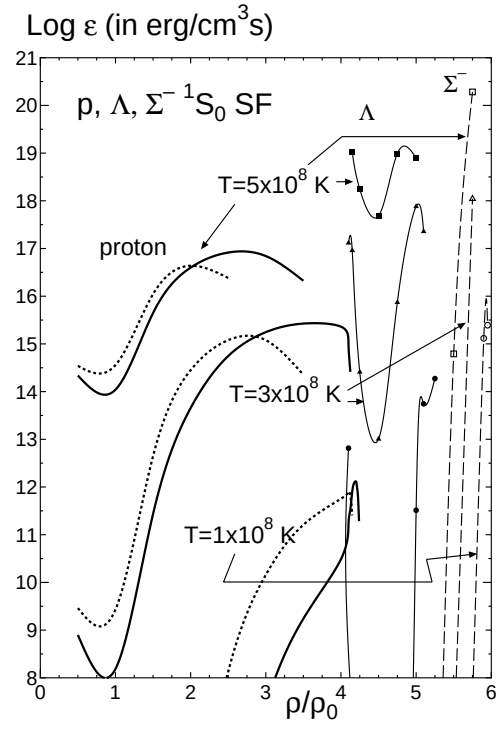

Fig. 15. Emissivities of the Cooper-pair process arising in the $^1S_0$ SF at three temperatures. Bold solid (dotted) curves are $\mathcal{E}_{\rm Cpp}(p)$ for OPEG (AV18). The thin solid and dashed curves are $\mathcal{E}_{\rm Cpp}(\Lambda)$ and $\mathcal{E}_{\rm Cpp}(\Sigma^-)$, respectively.

where $T_8 \equiv T/10^8$ K.

Because the $^3P_2$ SF gaps are anisotropic, the emissivity $\mathcal{E}_{\rm Cpp}(n)$ is affected by the angle dependence of the energy gaps, and $\mathcal{E}_{\rm Cpp}(n)$ differs for the two types with $m_J = 0$ and $|m_J| = 2$. This difference comes from the angular integrals giving the $F_t(n)$ functions in Eq. (5·12), because the magnitudes of two gaps are almost same. Due to the exponential in the denominator, the integral for the $m_J = 0$ gaps without a node on the Fermi surface is smaller than that for $|m_J| = 2$ gaps with nodes at the poles. Therefore $\mathcal{E}_{\rm Cpp}(n)$ for $m_J = 0$ is smaller than that for $|m_J| = 2$.

The calculated results are shown for $T = (1, 3, 5) \times 10^8$ K and for three potentials in Fig. 14. The bold curves represent $\mathcal{E}_{\rm Cpp}(n)$ for $m_J = 0$, and the thin curves are $\mathcal{E}_{\rm Cpp}(n)$ for $|m_J| = 2$. As is expected, the emissivities for $m_J = 0$ are smaller than those for $|m_J| = 2$, as clearly seen for $T = 1 \times 10^8$ K. The correspondence to the potentials is shown by the dotted (AV18), solid (OPEG-A) and dashed (OPEG-B). At $T = 1 \times 10^8$ K, we can see the clear difference depending on the magnitude of the energy gaps; the larger the energy gap, the smaller the emissivity. As T increases, this difference becomes less pronounced, but the difference in the density region

where $\mathcal{E}_{\rm Cpp}(n)$ is nonvanishing appears clearly in accordance with the width of the region where the $^3P_2$ SF exists [$T_c(n) > T$]. It is widest for OPEG-B, middle for OPEG-A and narrowest for AV18. When $T \gtrsim 8 \times 10^8$ K, the emissivity vanishes completely.

$\mathcal{E}_{\rm Cpp}$ from the proton $^1S_0$ SF The Cpp emissivity arising in the proton $^1S_0$ SF is given as [in units of erg/(cm^{3}s)]

$$\mathcal{E}_{Cpp}(p) = 4.72 \times 10^{11} T_8^7 (k_F(p)/\mathrm{fm}^{-1}) m_p^* F_s(p). \tag{5·16}$$

The calculated results are shown at $T = (1, 3, 5) \times 10^8$ K and for two potentials in Fig. 15. The bold solid (dotted) curves are obtained using the OPEG (AV18) potential. Because of the small reaction constants, $\mathcal{E}_{\rm Cpp}(p)$ is smaller than the modified Urca emissivity without SF suppression by at least one order of magnitude and much smaller than $\mathcal{E}_{\rm Cpp}(n)$. Also, the contributions are limited in the region where the proton $^1S_0$ SF exists, i.e. $\rho \lesssim 4\rho_0$. At $T = 1 \times 10^8$ K, up to baryon density $\rho \lesssim 3.5\rho_0$ where $T_c(p) \gtrsim 5T$, the proton gap strongly suppresses $\mathcal{E}_{\rm Cpp}(p)$, while at $T \gtrsim 3 \times 10^8$ K $\mathcal{E}_{\rm Cpp}(p)$ spread over $\rho \lesssim 4\rho_0$.

5.3.3. Hyperon sector

The formulas for the Cpp emissivity in the hyperon sector, where SF is of the $^1S_0$ pairing, are the same as those for the proton case, but the reaction constants are different. Concerning the reaction constants for Λ, there has been reported a mistaken statement that the Λ (also Σ^0) does not couple with the neutral current (NC) of the weak interaction.[27),28),13)] First of all this should be corrected before numerical calculations.

On the basis of TTT03, we use the correct expressions of the vector and axial vector coefficients, C_V and C_A. The proper choice of the quark NC[61)] naturally leads to the inclusion of the part originating from the GIM term of the quark NC ($J_\mu^{\rm GIM}$) in addition to the quark flavor $SU(3)$ octet term ($J_\mu^{\rm octet}$). The matrix elements of $J_\mu^{\rm octet}$ for Λ and Σ^0 vanish, while those of $J_\mu^{\rm GIM}$ do not. The mistaken statement stems from overlooking $J_\mu^{\rm GIM}$. For the nucleon, this does not contribute, because $J_\mu^{\rm GIM}$ is described by the s quark operator only. Thus, the correct expressions needed in the present study are: $C_V(\Lambda) = -1$, $C_V(\Sigma^-) = -(3 - 4\sin^2\theta_{\rm W}) = -2.08$, $C_A(\Lambda) = -(D/3 + F) + \Delta\Sigma = -0.61$, and $C_A(\Sigma^-) = D - 3F + \Delta\Sigma = -0.48$, where $D = 0.80$, $F = 0.47$ and $\Delta\Sigma = 0.127$ are chosen. C_V and C_A of the other octet baryons, except n and p, should be corrected. The resulting reaction constants for the Cpp process are summarized in Table III of Appendix D.

We have the following reaction constants for Λ and Σ^- arising in the $^1S_0$ SF:

$$a(\Lambda) = C_V(\Lambda)^2 = 1, \quad a(\Sigma^-) = C_V(\Sigma^-)^2 = 4.33. \tag{5·17}$$

The emissivities of Cpp for Λ and Σ^- are described in the same way as in the proton case, with $R(i) = a(i)F_s(i)$ ($i = \Lambda,\ \Sigma^-$). The results are shown in Fig. 15 with the solid thin curves for Λ and with the dashed curves for Σ^-. At $T = 1 \times 10^8$ K, because the $^1S_0$ SF gaps strongly suppress the emissivities, $\mathcal{E}_{\rm Cpp}(\Lambda)$ becomes appreciable only at the densities where the energy gap just starts ($\rho \simeq 4.0\rho_0 - 4.1\rho_0$) and fades away

($\rho \simeq 5.0\rho_0 - 5.2\rho_0$). $\mathcal{E}_{\rm Cpp}(\Sigma^-)$ is completely suppressed, except $\rho \simeq 5.7\rho_0 - 6.0\rho_0$, where the gap tends to vanish. Peak values of these emissivities are comparable with $\mathcal{E}_{\rm Cpp}(n)$, but the active regions are very narrow, and their contributions to the luminosity are expected to be small. As T increases, the active regions become wider, but the emissivities are still much smaller than $\mathcal{E}_{\rm Cpp}(n)$.

5.4. *Comparison of emissivities and discussion*

Now we can compare the efficient neutrino emissivities of the hyperon DUrca, the nucleon MUrca and the Cooper-pair processes. The main results are compiled in Fig. 16 at two internal temperatures, (a) $T = 1 \times 10^8$ K and (b) $T = 3 \times 10^8$ K. Here we omit some emissivities, which can be easily inferred from the figures given in the previous sections. The nucleon MUrca $\mathcal{E}_{\rm MU}$ only for OPEG-A is shown and the Cpp emissivity of the proton (hyperon) is not shown because it is much smaller than the more efficient $\mathcal{E}_{\rm Cpp}(n)$ ($\mathcal{E}_{\rm DU}$). The situation for the associated matter, superfluids (SFs) or normal, is indicated inside the figure. In addition, an example for the direct Urca emissivity in the presence of the charged-pion condensates is illustrated for discussion given below. The following points are to be noted:

1. At low and intermediate densities ($0.5\rho_0 \lesssim \rho \lesssim 4\rho_0$), the Cooper-pair process in the neutron $^3P_2$ SF dominates, being (1-2) orders of magnitude larger than the normal value of the nucleon $\mathcal{E}_{\rm MU}$ in most cases. Reflecting the different features of the $T_c(n)$ of the $^3P_2$ SF by the pairing potentials, the neutron $\mathcal{E}_{\rm Cpp}$ varies in (1-2) orders of magnitude at $T \simeq 1 \times 10^8$ K, while its active density regions vary at $T \simeq (3-5) \times 10^8$ K. Although its magnitude is still intermediate, the active density region is rather wide, especially for the potentials giving large $T_c(n)$, and the contribution to the luminosity is expected to be large.
2. At higher densities ($4\rho_0 \lesssim \rho \lesssim 6\rho_0$), the direct $\Lambda \leftrightarrow p$ Urca process dominates if $T_c(\Lambda) \lesssim 1 \times 10^9$ K, while it is completely suppressed if $T_c(\Lambda) \gg 1 \times 10^9$ K. The direct $\Sigma^- \leftrightarrow \Lambda$ URca process is active only if the NS mass M is large enough to have a central density with $\rho_c \gtrsim 5.5\rho_0$ for $M \gtrsim 1.5 M_\odot$ for TNI6u-EOS. For $T_c(\Lambda) \lesssim T$, $\mathcal{E}_{\rm DU}(\Lambda \leftrightarrow p)$ is very large near the value for the normal Λ matter. In such a case, the NS mass M plays a crucial role as to whether the central density exceeds the onset density of Λ or not, namely, $\rho_c \simeq 4\rho_0$ or not, for TNI6u-EOS.
3. We have studied the features of the neutrino emissivities without a meson condensate which provides the *nonstandard* cooling. For meson condensates, the charged-pion condensation has the most important relevance to the present context, because it provides the pion Durca emissivity and also its onset density is considered to be $\rho_t(\pi^c) \simeq (2.0 - 2.5)\rho_0$. Many works have been done on this problem,[62)–66)] but there are still unsolved problems to be studied further. The recent study based on laboratory experiments on the spin-isosin excitation of nuclei[67),68)] suggests that the onset densities of both the neutral- and charged-pion condensations are even lower than the value mentioned above. A large emissivity from the pion-DUrca process comes about for $\rho \gtrsim 2\rho_0$. If the superfluid gap vanishes or is small, the emissivity is given by the large values indicated

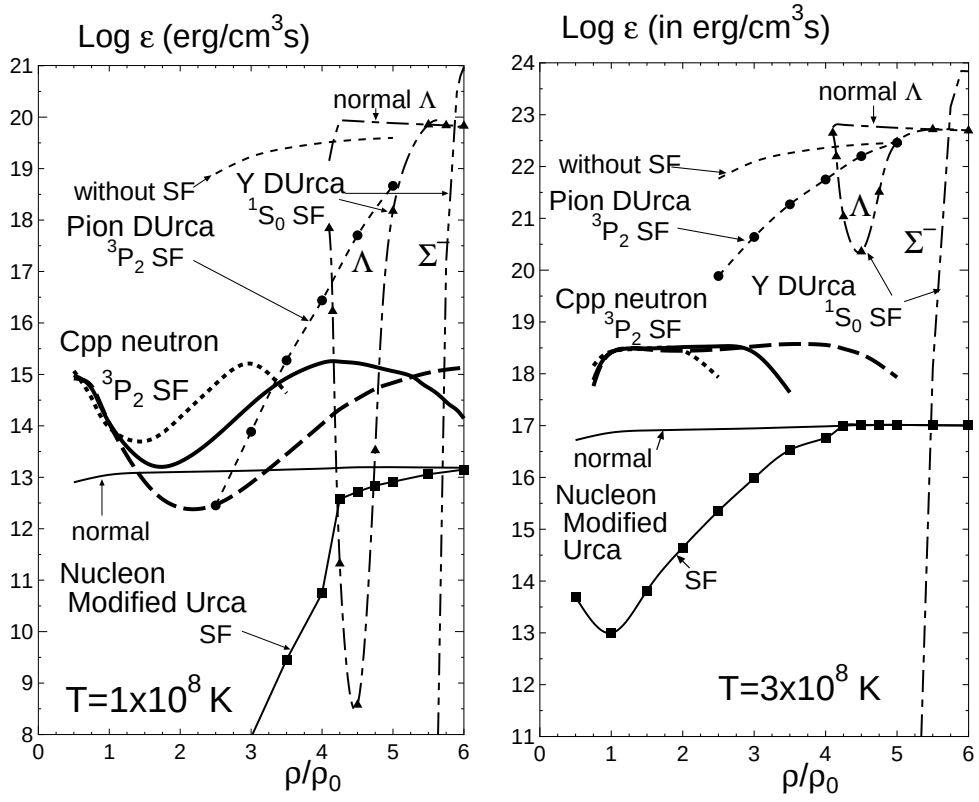

Fig. 16. Comparison of three efficient neutrino emissivities as functions of density: (a) at $T = 1 \times 10^8$ K and (b) at $T = 3 \times 10^8$ K, where minor contributions are omitted. The bold dotted, solid and dashed curves represent $\mathcal{E}_{\rm Cpp}$ in the neutron ${}^3P_2(m_J = 0)$ SF for the AV18, OPEG-A and OPEG-B potentials, respectively. The solid curve with (without) squares represents $\mathcal{E}_{\rm MU}$ in the neutron ${}^3P_2$ and proton ${}^1S_0$ SFs (normal n, p). The Dash-dot curve with (without) triangles shows $\mathcal{E}_{\rm DU}$ in Λ ${}^1S_0$ SF (normal Λ) for Λ decay. The dash-dot-dot vertical line shows $\mathcal{E}_{\rm DU}$ for Σ^- decay. The short dashed curve with (without) circles illustrates an example of the emissivity of pion direct Urca for charged-pion condensed quasi-nucleon matter with (without) SF suppression.

by the short-dashed curves in Fig. 16, being of the same order as $\mathcal{E}_{\rm DU}(\Lambda \leftrightarrow p)$ for the normal Λ matter. The short-dashed curves with the filled circles in Fig. 16 show an example of the emissivity for the existence of the ${}^3P_2$ SF of the quasi-nucleons (in a particular mixed state of the nucleon and the Δ-isobar due to the pion condensation, which we have denoted as an η-particle[63),65)]) with a moderate SF energy gap which is an optimum case among those hitherto studied.[69)] The resulting emissivity increases as the density increases, because the critical temperature of the η-particle decreases gradually. Clearly, the pion direct Urca is a candidate as an agent of *nonstandard* NS cooling if a suitable SF coexists.[9)] Concerning this point, we need further study on the superfluidity of the baryons accompanying the Δ mixing under the combined pion conden-

sation, where the charged and neutral pion condensates coexist.*)

§6. Summary and concluding remarks related to neutron star cooling

We studied the features of neutron star matter with hyperon mixing whose maximum mass compatible with observations is assured by introducing the universal repulsive three-body force. In this study, we treated the case without a meson condensate. With the equation of state obtained by this interaction model (which we call TNI6u-EOS), we obtained the composition of particles which leads to the following important features of the neutron star matter: The mixing of Λ and Σ^- starts at $\simeq 4\rho_0$, the nucleon direct Urca process does not occur up to $\simeq 6.5\rho_0$ and the hyperon direct Urca process is possible only for the $\Lambda \leftrightarrow p$ and the $\Sigma^- \leftrightarrow \Lambda$ transitions. The critical temperatures of the baryon superfluids (the neutron $^3P_2$ pairing and the $^1S_0$ pairing of p, Λ and Σ^-), were obtained by the pairing interaction carefully chosen with a reliable allowance, and their density dependence provides the basic nuclear physics inputs for calculations of neutrino emissivities. For the temperature dependence of the energy gap, we obtained the profile functions are independent of the background (densities, effective masses and pairing interactions) for the proton $^1S_0$ pairing and the neutron $^3P_2$ pairing.

The neutrino emissivities of three processes efficient in the neutron star core, the hyperon direct Urca, the nucleon modified Urca and the Cooper-pair processes, were calculated. After the emissivity of each process was studied, main features of the results were presented and a comparison was made. In the last part of the previous section we summarized the main features. At low and intermediate densities ($\rho \lesssim 4\rho_0$), the Cooper-pair emissivity arising from the neutron $^3P_2$ superfluid dominates. At higher densities ($\rho \gtrsim 4\rho_0$) the emissivity of the $\Lambda \leftrightarrow p$ direct Urca dominates, but its magnitude depends strongly on the $^1S_0$ energy gap of Λ which reflects sensitively the attractive feature of the $\Lambda\Lambda$ interaction acting in double Λ hypernuclei.

In the course of the present study, we have revised the T72 results of the zero-temperature energy gap of the $^3P_2$ pairing in pure neutron matter, which was reported in 1972.[43] We presented the new expressions for the reaction constants for the hyperon Cooper-pair process, after correcting a mistaken statement appeared previously that the neutral current of the weak interaction does not couple to Λ and Σ^0.

The features of the emissivities for neutron stars (NSs) with and without hyperon-mixed core have been taken into account in recent calculations performed by Tsuruta and her collaborators[71] concerning the thermal evolution of NSs. The thermal evolution curves describe the change of surface photon luminosity (L) corresponding to surface temperature as a function of age of neutron stars (t). Comparison of the calculated results with the observational data leads to the following points to be

*) The study in Ref. 9) was performed with use of the SF critical temperatures under the pion condensation, which is based on the results of a simple model approach done in 1980-82[70] and is extended phenomenologically to high density region.

noted:

1. The colder class NS data ($L^{\rm obs} \sim 10^{33\to31.5}$ erg/s for $t = 10^{3\to5.5}$ years) are reproduced well by taking a neutron star mass $M \simeq (1.5-1.6)M_\odot$ with the hyperon-mixed core providing the neutrino emission due to the hyperon direct Urca process, if suppressed properly by the Λ $^1S_0$ superfluid with its critical temperature $T_c^{(\Lambda)} \sim 10^9$ K. If we take a less attractive $\Lambda\Lambda$ interaction leading to $T_c^{(\Lambda)} \lesssim$ [internal temperature], we face such serious contradiction with observations that all the colder class NSs are too cold to be observed.
2. The hotter class NS data ($L^{\rm obs} \sim 10^{34\to32}$ erg/s for $t = 10^{3\to6}$ years) can be reproduced by taking a neutron star mass $M \lesssim 1.4M_\odot$ without the hyperon-mixed core, since the cooling effect due to the Cooper-pair process is qualitatively in balance with the effect due to the vortex creep heating with a heating parameter of the order of $K = 10^{37}$erg m$^{-3/2}$s^2. [10]
3. The small $\Lambda\Lambda$-bond energy in ${}^{6}_{\Lambda\Lambda}$He suggested by "NAGARA" event [56] leads to a vanishing energy gap of Λ, if this feature is attributed only to the decrease of the $\Lambda\Lambda$ $^1S_0$ attraction. Then, the NSs with the hyperon-mixed core become unobservable due to the very large emissivity of the direct $\Lambda \leftrightarrow p$ Urca process, and the hyperon-mixed core cannot be a candidate responsible for the *nonstandard* cooling. In the context of NS cooling, therefore, it is important to study the possibility that this aspect provided by the "NAGARA" event is explained without reduction of the $\Lambda\Lambda$ $^1S_0$ attraction, e.g. by introducing a repulsive $\Lambda\Lambda N$ three-body interaction and some many-body effect not explored yet.
4. If meson condensation takes place, it gives rise to strong direct Urca coolingand leads to too rapid cooling, if superfluid suppression is absent or weak. Therefore, the persistence of baryon SF in the meson-condensed phase is necessary. Since realization of pion condensation is expected above about twice the nuclear density, it is important to confirm the persistence of the superfluid under the pion condensed phase that has the energy gap large enough to give a moderately strong suppression to the pion direct Urca emissivity.

Acknowledgements

The authors wish to thank S. Nishizaki and Y. Yamamoto for their collaboration in studies on hyperon-mixed neutron star matter and T. Tatsumi for his helpful discussions on the cooling problem. They also thank S. Tsuruta for cooperative discussions and sending us her Sydney Conference paper before publication.

Appendix A

—— On NN Potentials Adopted as the Pairing Interaction ——

Here we mention detailed properties of the NN potentials adopted as the pairing interaction in this paper. OPEG potential [24] is of the charge-independent v-14 type and is given by the following five terms:

$$V(1,2) = V_C + S_{12}V_T + (\boldsymbol{L}\cdot\boldsymbol{S})V_{LS} + W_{12}V_W + \boldsymbol{L}^2 V_{LL}, \tag{A·1}$$

where two-nucleons are denoted by 1 and 2. $\boldsymbol{L}$ ($\boldsymbol{S}$) is the relative orbital (total spin) angular momentum in unit of $\hbar$. S_{12} is the tensor operator and W_{12} is the quadratic spin-orbit operator whose matrix elements are given by

$$W_{12} = (\boldsymbol{L}\cdot\boldsymbol{S})^2 - \{\delta_{L,J} + \boldsymbol{\sigma}_1\cdot\boldsymbol{\sigma}_2/3\}L(L+1),$$

with the magnitude of the orbital (total) angular momentum L (J). Also, the quantities V_a with $a = C$, T, LS, W and LL are functions of the internucleon distance r, which are given for each state with spin S and isospin T (or equivalently, parity Π). The potential has no explicit momentum dependence, and the momentum dependence is involved only in $\boldsymbol{L}$ implicitly.

AV18[23] is one of the modern charge-dependent NN potentials which contains the charge dependence (CD) in the static OPEP through its pion masses, the CD from the electromagnetic interaction and the CD in the central term of nuclear interaction restricted to the S-wave. The nuclear part of AV18 is defined as

$$V(1,2) = v^c + v^{l2}\boldsymbol{L}^2 + v^t S_{12} + v^{ls}(\boldsymbol{L}\cdot\boldsymbol{S}) + v^{ls2}(\boldsymbol{L}\cdot\boldsymbol{S})^2. \tag{A·2}$$

Because $(\boldsymbol{L}\cdot\boldsymbol{S})^2$ is related to W_{12} as

$$(\boldsymbol{L}\cdot\boldsymbol{S})^2 = \frac{1}{2}W_{12} + \frac{2}{3}\boldsymbol{L}^2 - \frac{1}{2}(\boldsymbol{L}\cdot\boldsymbol{S}), \tag{A·3}$$

the following relations hold:

$$V_{LS} = v^{ls} - v^{ls2}/2, \quad V_W = v^{ls2}/2, \quad V_{LL} = v^{l2} + 3v^{ls2}/2. \tag{A·4}$$

In the neutron star matter, the electrons and muons making the negative-charge background smear out most of the effects from the electric field including the Coulomb potential between protons. In calculations for NS matter, therefore, we use only the nuclear part of the nn potential of AV18 as the nuclear part of the pp potential, because of the good charge symmetry in NN interaction. In this paper we treat the pp ${}^1S_0$ and the nn ${}^3P_2 + {}^3F_2$ interactions. OPEG have two versions (A and B) in the ${}^3P_2 + {}^3F_2$ state, but they are the same in the ${}^1S_0$ state.

In the ${}^1S_0$ state, AV18 and OPEG give almost the same scattering phase shifts in the elastic region. If we extend calculations to the inelastic region using the NN channel only, AV18 gives somewhat lower phase shifts than those by OPEG (e.g., about 5 degrees at $T_{\rm Lab} = 600$ MeV), because it has a stronger repulsive core and a slightly deeper attraction just outside the core than OPEG, in this state.

In the ${}^3P_2 + {}^3F_2$ state, we adopt three potentials, AV18, OPEG-A and OPEG-B whose repulsive cores become weaker in this order. Although these three potentials give almost the same scattering phase shifts and mixing parameters in the elastic region, they give different ${}^3P_2$ phase shifts $\delta({}^3P_2)$ for $T_{\rm Lab} \gtrsim 400$ MeV, as shown in Fig. 4, if we extend calculations using the NN channel only. The largest $\delta({}^3P_2)$ shown for OPEG-B are near those given by the CD-Bonn potential[34] at such $T_{\rm Lab}$.

These values thus obtained are the so-called background phase shifts, upon which effects of open channels are superimposed. Therefore, the broad hump-like behavior of $\delta(^3P_2)$ seen for $T_{\rm Lab} \gtrsim$500 MeV is not to be explained by the NN potential only, but to be explained by the resonance-like effects reflecting the $N\Delta$ state in the $NN\pi$ channel. There is no reason to regard such a potential yielding high values to $\delta(^3P_2)$ for $T_{\rm Lab} \gtrsim$500 MeV (e.g., like Nijmegen I, II [72]) as realistic. We regard the variety seen in the three potentials (AV18,OPEG-A and OPEG-B) as a reliable allowance in the $^3P_2$ pairing interaction.

Appendix B

—— Relations in NFSA (Near-Fermi Surface Approximation) Used in the Text ——

Here, we treat three energy gaps at the Fermi surface for temperature T, which are denoted in §3 by $(\Delta,\ \Delta_0,\ \Delta_2)$ for the ($^1S_0$, $^3P_2$ with $m_J=0$, $^3P_2$ with $|m_J|=2$), in a parallel way. There, we have written the relations of the effective critical temperature T_c^* to the zero temperature energy gap as

$$k_B T_c^* = (0.57\Delta(k_F, T=0),\ 0.60\Delta_0(k_F, T=0),\ 0.61\Delta_2(k_F, T=0)). \tag{B·1}$$

The coefficients denoted as a_0^* in §4 are given in NFSA as follows. By solving the gap equation in a small interval $\epsilon_k - \epsilon_F = (-\xi, +\xi)$ with the effective partial-wave pairing matrix element $\langle k_F|\tilde{V}_\lambda|k_F\rangle$, we have the well-known equation

$$k_B T_c^* \simeq 1.14\ \xi\ \exp(-1/\rho(0)U_\lambda), \tag{B·2}$$

where $\rho(0) = M^* k_F/2\pi^2\hbar^2$ and $U_\lambda \equiv -4\pi\langle k_F|\tilde{V}_\lambda|k_F\rangle$. The zero temperature energy gaps are obtained as

$$(\Delta,\ \sqrt{4\pi}\Delta_0,\ \sqrt{4\pi}\Delta_2)_{k_F,T=0} = 2\xi\ (1,\ \Gamma_0,\ \Gamma_2) \times \exp(-1/\rho(0)U_\lambda), \tag{B·3}$$

where $\Gamma_0 = 3.39$ and $\Gamma_2 = 3.32$. These numbers come from the angle dependence of the gaps: $\ln\Gamma_{|m_J|} \equiv -\int d\Omega_k f(\theta_k)^2\ \ln f(\theta_k)$ with $\sqrt{4\pi} f(\theta_k) = \Theta_{|m_J|}(\theta_k)$ used in Eqs. (3·4). Eliminating ξ from (B·2) and (B·3) we obtain the relation (B·1).

The behavior of the energy gap near T_c is obtained by studying the thermodynamic potential near T_c (T_c^* in our sense):

$$\Delta(k_F, T) \simeq \sqrt{\frac{8\pi^2}{7\zeta(3)}} k_B T_c^* \left(1 - \frac{T}{T_c^*}\right)^{1/2} = 3.06\ a_0^*\ \Delta(k_F, 0) \left(1 - \frac{T}{T_c^*}\right)^{1/2}, \tag{B·4}$$

where ζ is the zeta function, as is well known in the $^1S_0$ case. [49),50)] Similarly, we have

$$\Delta_{|m_J|}(k_F, T) \simeq \sqrt{\frac{20\pi^2}{21\zeta(3)}} k_B T_c^* \left(1 - \frac{T}{T_c^*}\right)^{1/2} = 2.80\ a_0^*\ \Delta_{|m_J|}(k_F, 0) \left(1 - \frac{T}{T_c^*}\right)^{1/2} \tag{B·5}$$

for the $^3P_2$ pairing. The coefficients (3.06 and 2.80) correspond to the values of C_1 appearing in Eq. (4·1c), which are obtained in NFSA and are the same as those used in Ref. 51).

The limiting form for $\tau \to 0$ of Eq. (4·1b) is the familiar one for the $^1S_0$ pairing. For the $^3P_2$ pairing too, the same form is obtained if we use the angle average approximation in the procedure in deriving the limiting form. A quality test of this approximation done numerically shows that it is fairly good, as the errors are at most about 5%.

Appendix C

—— On Construction of Profile Function to Describe the Temperature Dependence of the Energy Gap ——

Here, the numerical basis for the construction of the profile functions $P(\tau)$ describing the temperature dependence of energy gaps is explained. In Table II we give the average and the spread of the deviation from the average for the ratios $\Delta(k_F, T)/\Delta(k_F, T = 0)$ in the $^1S_0$ calculated over the 12 proton fractional densities with y_p and the proton effective mass parameter m_p^* under TNI6u-EOS for the two potentials indicated. Similarly, for the three pairing potentials indicated, we give the same quantities on the ratios $\Delta_{|m_J|}(k_F, T)/\Delta_{|m_J|}(k_F, T = 0)$ for the $^3P_2$ pairing with $m_J = 0$ ($|m_J| = 2$), which are obtained by solving the $^3P_2 + {}^3F_2$ coupled gap equation (the uncoupled $^3P_2$ gap equation) over 9 densities in pure neutron matter with m_n^* as explained in the text.

Table II. Average and spread of deviation from the average taken for the ratios of the calculated energy gaps at T to those at $T = 0$ for each $\tau = T/T_c$ and for the pairing type and the potential, indicated in the first row. Here [0] and [2] represent $|m_J|$. In each frame, the upper (lower) number is the average (spread).

Case	$^1S_0$	$^1S_0$	$^3P_2$ [0]	$^3P_2$ [0]	$^3P_2$ [0]	$^3P_2$ [2]	$^3P_2$ [2]	$^3P_2$ [2]
τ	AV18	OPEG	AV18	OPEG-A	OPEG-B	AV18	OPEG-A	OPEG-B
0.3	0.9970	0.9970	0.993	0.992	0.992	0.992	0.992	0.992
	0	0	1	1	1	0	0	0
0.5	0.9558	0.9558	0.938	0.938	0.939	0.938	0.938	0.938
	1	2	1	2	3	1	0	0
0.7	0.8250	0.8250	0.797	0.795	0.797	0.790	0.790	0.790
	4	6	4	4	3	1	2	1
0.8	0.7046	0.7046	0.673	0.668	0.671	0.657	0.658	0.656
	8	10	7	7	5	1	3	2
0.9	0.5141	0.5141	0.477	0.467	0.474	0.441	0.432	0.439
	16	20	13	13	10	5	8	5
0.95	0.3603	0.3604	0.314	0.297	0.312	0.251	0.250	0.244
	27	33	23	24	14	20	23	18
0.97	0.270	0.270	0.213	0.195	0.204	0.116	0.108	0.097
	4	5	35	29	28	53	56	51

Appendix D

—— Reaction Constants for the Cooper-Pair Process ——

The reaction constants $a(i)$ of the Cooper pair process are given in Table III. These values were obtained on the basis of C_V and C_A for the octet baryon (i) given

in the tables of TTT03.[26] Chosing $D = 0.80$, $F = 0.47$ and $\Sigma = 0.23$, we use $g_A \equiv D + F = 1.27$ and $\Delta\Sigma \equiv -D/3 + F - \Sigma = 0.13$, together with $\sin^2\theta_W = 0.23$.

Table III. Reaction constants of the Cooper-pair process.

Baryon	Pairing	$a(i)$
n, Ξ^0	$^1S_0$	1
n	$^3P_2$	$1 + 2(-g_A + \Delta\Sigma)^2 = 3.60$
p, Σ^+	$^1S_0$	$(1 - 4\sin^2\theta_W)^2 = 0.0064$
p	$^3P_2$	$(1 - 4\sin^2\theta_W)^2 + 2(g_A + \Delta\Sigma)^2 = 3.93$
Σ^-, Ξ^-	$^1S_0$	$(3 - 4\sin^2\theta_W)^2 = 4.33$
Λ, Σ^0	$^1S_0$	1

References

1) S. Nishizaki, Y. Yamamoto and T. Takatsuka, Prog. Theor. Phys. **108** (2002), 703. This paper is referred to as NYT02.
2) I. E. Lagaris and V. R. Pandharipande, Nucl. Phys. A **359** (1981), 349.
3) H. Heiselberg and V. Pandharipande, Ann. Rev. Nucl. Part. Sci. **50** (2000), 481.
4) S. Tsuruta, Comments Astrophys. **11** (1986), 151.
5) D. Page and E. Baron, Astrophys. J. **354** (1990), L17.
6) S. Tsuruta, *Proc. US-Japan Joint Seminar on "The Structure and Evolution of Neutron Stars", Kyoto, 1990*, ed. D. Pines, R. Tamagaki and S. Tsuruta (Addison-Wesley, 1992), p. 371.
7) D. Page and J. H. Applegate, Astrophys. J. **394** (1992), L17.
8) J. M. Lattimer, K. A. Van Riper, M. Prakash and M. Prakash, Astrophys. J. **425** (1994), 802.
9) H. Umeda, K. Nomoto, S. Tsuruta, T. Muto and T. Tatsumi, Astrophys. J. **431** (1994), 309.
10) H. Umeda, S. Tsuruta and K. Nomoto, Astrophys. J. **433** (1994), 256.
11) C. J. Pethick, Rev. Mod. Phys. **64** (1992), 1133.
12) S. Tsuruta, Phys. Rep. **292** (1998), 1.
13) D. G. Yakovlev, A. D. Kaminker, O. Y. Gnedin and P. Haensel, Phys. Rep. **351** (2001) 1.
14) T. Takatsuka and R. Tamagaki, Prog. Theor. Phys. **97** (1997), 345.
15) T. Takatsuka and R. Tamagaki, Prog. Theor. Phys. **94** (1995), 457.
16) O. V. Maxwell, Phys. Rev. **231** (1979), 201.
17) E. Flowers, M. Ruderman and P. Sutherland, Astrophys. J. **205** (1976), 541.
18) A. D. Kaminker, P. Heansel and D. G. Yakovlev, Astron. Astrophys. **373** (2001), L17.
19) D. G. Yakovlev, A. D. Kaminker and O. Y. Gdenin, Astron. Astrophys. **379** (2001), L5.
20) D. G. Yakovlev and P. Heansel, Astron. Astrophys. **407** (2003), 259.
21) S. Tsuruta, M. A. Teter, T. Takatsuka, T. Tatsumi and R. Tamagaki, Astrophys. J. **571** (2002), L143.
22) T. Takatsuka, S. Nishizaki, Y. Yamamoto and R. Tamagaki, in preparation.
23) R. B. Wiringa, V. G. Stoks and R. Schiavilla, Phys. Rev. C **51** (1995), 38.
24) R. Tamagaki and T. Takatsuka, Prog. Theor. Phys. **105** (2001), 1059. R. Tamagaki, Prog. Theor. Phys. **39** (1968), 91.
25) T. Takatsuka, S. Nishizaki, Y. Yamamoto and R. Tamagaki, Few-body Systems Suppl. **12** (2000), 108.
26) T. Tatsumi, T. Takatsuka and R. Tamagaki, Prog. Theor. Phys. **110** (2003), 179. This paper is referred to as TTT03.
27) O. V. Maxwell, Astrophys. J. **316** (1987), 691.
28) D. G. Yakovlev, A. D. Kaminker and K. P. Levenfish, Astron. Astrophys. **343** (1999), 650. This paper is referred to as YKL99.
29) Preliminary report of this paper: T. Takatsuka and R. Tamagaki, *Proc. Int. Conf. on "Clustering Aspects of Nuclear Structure and Dynamics"*, ed K. Ileda, I. Tanihata and H. Horiuchi, Nucl. Phys. A **738** (2004), C387.

30) Y. Yamamoto, S. Nishizaki and T. Takatsuka, Prog. Theor. Phys. **103** (2000), 981.
31) V. G. J. Stoks, R. A. M. Klomp, M. C. M. Rentmeester and J. J. de Swart, Phys. Rev. C **48** (1993). 792.
32) R. A. Arndt, Scattering Analysis Interactive Dial-up; SAID (2001).
33) R. A. Arndt, J. S. Hyslop III and L. D. Roper, Phys. Rev. **35** (1987), 128.
34) R. Machleidt, Phys. Rev. **63** (2001), 024001.
35) T. Takatsuka, S. Nishizaki, Y. Yamamoto and R. Tamagaki, Prog. Theor. Phys. **105** (2001), 179.
36) T. Takatsuka, S. Nishizaki, Y. Yamamoto and R. Tamagaki, Prog. Theor. Phys. Suppl. No. 146 (2002), 279.
37) T. Takatsuka and R. Tamagaki, Nucl. Phys. A **721** (2003), 1003C.
38) J. M. C. Chen, J. W. Clark, E. Krotscheck and R. A. Smith, Nucl. Phys. A **451** (1986), 509.
T. L Ainsworth, J. Wambach and D. Pines, Phys. Lett. B **222** (1989), 173.
U. Lombardo and H. J. Schulze, *Lecture Notes in Phys.* **578**, ed. D. Blaschke, N. K. Glendening and A. Sedtrakian (Springer, 2001), p. 30, and related references cited therein.
39) T. Takatsuka and R. Tamagaki, Prog. Theor. Phys. **46** (1971), 114.
40) R. Tamagaki, Prog. Theor. Phys. **44** (1970), 905.
41) M. H. Hoffberg, A. E. Glassgold, R. W. Richardson and M. Ruderman, Phys. Rev. Lett. **24** (1970), 775.
42) D. G. Yakovlev, K. P. Levenfish and Yu. A. Shibanov, Physics-Uspehki **42** (1999), 737. (Translated from Usp. Fiz. Nauk **169** (1999), 825.)
43) T. Takatsuka, Prog. Theor. Phys. **47** (1972), 1062; Prog. Theor. Phys. **48** (1972), 1517. This paper is referred to as T72.
44) T. Takatsuka and R. Tamagaki, Prog. Theor. Phys. Suppl. No. 112 (1993), 27.
45) M. Baldo, Ø. Elgarøy, L. Engvik, M. Hjorth-Jensen and H. -J. Schulze, Phys. Rev. C **58** (1998), 1921.
46) A. D Jackson, E. Krotscheck, D. E. Meltzer and R. A. Smith, Nucl. Phys. A **386** (1982), 125.
47) A. Schwenk and B. Friman, Phys. Rev. Lett. **92** (2004), 082501.
48) V. A. Kohdel, J. W. Clark, M. Takano and M. Zverev, astro-ph/042514.
49) S. Nakajima, *Introduction to Superconductivity*, in Japanese (Baifukan, Tokyo, 1971).
50) A. L. Fetta and J. D. Walecka, *Quantum Theory of Many Particle Systems* (McGraw-Hill, New York, 1971).
51) K. P. Levenfish and D. G. Yakovlev, Astron. Rep. **38** (1994), 247. (Translated from Astron. Zh. **71** (1994), 282.)
52) T. Takatsuka and R. Tamagaki, Prog. Theor. Phys. **97** (1997), 203; Prog. Theor. Phys. **99** (1998), 161.
53) M. Prakash, M. Prakash, J. M. Lattimer and C. J. Pethick, Astrophys. J. **390** (1992), L77.
54) M. Prakash, Phys. Rep. **242** (1994), 297.
55) K. P. Levenfish and D. G. Yakovlev, Astron. Lett. **20** (1994), 43. (Translated from Pis'ma Zh. **20** (1994), 54.)
56) H. Takahashi et al., Phys. Rev. Lett. **87** (2001), 212502.
57) B. L. Friman and O. V. Maxwell, Astrophys. J. **390** (1992), L77.
58) M. E. Gusakov, Astron. Astrophys. **389** (2002), 702.
59) A. V. Senatorov and D. N. Voskresensky, Phys. Lett. **184** (1987), 119.
60) Ch. Schaab, D. Voskresensky, A. D. Sedrakian, F. Weber and M. K. Weigel, Astron. Astrophys. **321** (1997), 591.
61) T. D. Lee, *Particle Physics and Introduction to Field Theory* (Harwood Academic Pub., 1988).
62) O. V. Maxwell, G. E. Brown, D. K. Campbell, R. F. Dashen and J. T. Manassah, Astrophys. J. **216** (1977), 77.
63) T. Tatsumi, Prog. Theor. Phys. **69** (1983), 1137.
T. Muto and T. Tatsumi, Prog. Theor. Phys. **79** (1988), 461.
64) A. B. Migdal, E. E. Saperstein, M. A. Troitsky and D. N. Voskresensky, Phys. Rep. **192** (1990), 179.
65) T. Muto, R. Tamagaki and T. Tatsumi, Prog. Theor. Phys. Suppl. No. 112 (1993), 159,

and references cited therein.
66) T. Muto, T. Takatsuka, R. Tamagaki and T. Tatsumi, Prog. Theor. Phys. Suppl. No. 112 (1993), 221.
67) T. Suzuki and H. Sakai, Phys. Lett. **455** (1999), 25.
68) T. Suzuki, H. Sakai and T. Tatsumi, *Proc. RCNP Int. Symp. on "Nuclear Responces and Medium Effects"*, ed. T. Noro et al. (Universal Academy Press, 1999), p. 77.
T. Tatsumi, *Proc. Kyudai-RCNP Symp. on "Nuclear Many-Body and Medium Effects in Nuclear Interactions and Reactions"*, ed. K. Hatanaka et al. (World Scientific, 2003), p. 18.
69) T. Takatsuka and R. Tamagaki, Prog. Theor. Phys. **101** (1999), 1043.
70) T. Takatsuka and R. Tamagaki, Prog. Theor. Phys. **64** (1980), 2270; Prog. Theor. Phys. **67** (1982), 1649; Prog. Theor. Phys. Suppl. No. 112 (1993), 107.
71) S. Tsuruta, review paper presented at IAU Symposium, July 2003, Sydney.
72) V. G. Stoks, R. A. M. Klomp, C. P. F. Terheggen and J. J. de Swart, Phys. Rev. C **49** (1994), 2950.